Vol. 2 December, 1958 No. 5

MINERALOGICAL JOURNAL

CONTENTS

The Measurement of the Integrated Intensity by Means of a Single Crystal X-Ray Diffractometer ..... Y. Iitaka..... 283

Aluminian Serpentine and Associated Chlorite from Usagiyama, Fukuoka Prefecture, Japan ..... H. Shirozu..... 298

A Detailed Investigation of the Structure of Hexagonal $BaAl_2Si_2O_8$ with Reference to Its α-β Inversion..... ..... Y. Takéuchi..... 311

Short Communications

Lithian Biotite from the Takatori Mine, Ibaragi Prefecture ... . T, Kato..... 333

Abstract of the Kobutsugaku Zasshi, Journal of the Mineralogical Society of Japan, Vol. 3, No. 6..... 336

The Mineralogical Society of Japan

Department of Geology and Mineralogy, Faculty of Science, Hokkaido University, Sapporo, Japan

MINERALOGICAL JOURNAL

published by

The Mineralogical Society of Japan

EDITORIAL BOARD

Zyunpéi Harada, *Hokkaido University;* Teiichi Ito, *University of Tokyo;* (Chief) Nobuo Katayama, *University of Tokyo;* Keiichi Omori, *Tohoku University;* Ryôiti Kiriyama, *University of Osaka;* Seitaro Tsuboi, *University of Tokyo;* Takeo Watanabe, *University of Tokyo;* Toyofumi Yoshimura, *Kyushu University.*

Instructions to Contributors

Manuscripts of articles should be submitted to the executive editor, Nobuo Katayama, at the College of General Education, University of Tokyo, Komaba, Meguro-ku, Tokyo. The manuscript should be typewritten with double space lines, and not exceed 20 sheets of normal typewriting paper. References of literature should be in accordance with the forms used in the pages of this journal.

Plates and figures should be capable of reduction to not more than 10 by 15 centimetres. Line drawings should be in black India ink on white drawing board, tracing paper, or coordinate paper printed in blue. Photographs should be positive glossy prints.

Two referees chosen by the Editorial Board read the manuscript of article submitted before it is accepted for publication.

Thirty reprints without cover will be furnished to the author free of cost and without previous notice from him. Additional reprints will be furnished at cost when ordered.

The price of the journal to subscribers in Japan is 250 yen for a single copy (including postage), and to subscribers in other countries $ 1.00 (including postage) for a single copy, or $ 5.00 (including postage) per volume of 6 numbers.

Printed in Japan

Mineralogical Journal, Vol. 2, No. 5, pp. 283-297, Dec., 1958

THE MEASUREMENT OF THE INTEGRATED INTENSITY BY MEANS OF A SINGLE CRYSTAL X-RAY DIFFRACTOMETER

Yōichi Iitaka

Mineralogical Institute, University of Tokyo

Abstract

In the course of a study of the crystal structure of β-glycine a Geiger counter diffractometer was successfully utilized for the measurement of the integrated intensities from a single crystal. This paper describes the apparatus used and the method for measuring them. A proportional and a scintillation counter were tested for the measurement. A comparison has been made between these counters and their relative merits are discussed.

Introduction

The use of an X-ray diffractometer as a precision instrument for investigating the scattering from crystalline materials has become more widespread during the course of the last few years. However, most of the papers were concerned with the instruments designed primarily for recording powder patterns and the main problem is the measurement of the position, intensities and shapes of lines diffracted by powder specimens.

Recently, the application of the method to the study of single crystal specimens has been reported by many workers, where the main problem is the measurement of the thermal diffuse scattering of X-rays[6) 9) 10)] or the measurement of the integrated intensities of Bragg reflections[2) 3) 5) 8) 11)].

Since the quantum efficiency of the counter for X-rays may be made to approach 100%, a properly designed diffractometer must always give more sensitive and more accurate results than a

photographic method. Intensity measurement from a photograph is essentially indirect and is subject to a number of random experimental errors. Furthermore, it does not, in general, give the integrated intensity. Cochran[3] examined the accuracy of the photographic and Geiger counter methods of intensity measurement and showed that under practical conditions greater accuracy and sensitivity can be obtained for roughly the same time of measurement when the counter diffractometer rather than a Weissenberg camera is used in the investigation of small single crystals.

In this connection, we have constructed the instrument described below, for the accurate measurement of integrated intensities from small single crystals. The application of the method to the study of the crystal structure of β-glycine will be described in a later paper.

Apparatus

The apparatus shown in Fig. 1 (Plate I) was designed for accurate measurement of the integrated intensity of X-rays from a single crystal. A standard optical goniometer was modified into an X-ray goniometer by attaching an entrance slit system (E), an arm to carry the counter (C), and a driving mechanism (D) which rotates the counter arm at a constant angular velocity. The crystal was mounted on the goniometer head (G) which can be clamped to the shaft (O), (O) being geared to rotate at one half the speed of the counter arm. The angular position of the goniometer head can be read from the circular scale (R), and enables any desired plane to be brought into a reflecting position. The arm bearing the counter can be inclined to the horizontal plane for measurements of higher layer lines; but in the present study only the zero-layer reflections have been measured. With this apparatus it was possible to measure reflections at angles less than 150° (2θ). The entrance slit arrangement consisted of two slits S_1 and S_2, for collimating the incident beam. Another slit S_3 was mounted on the arm in

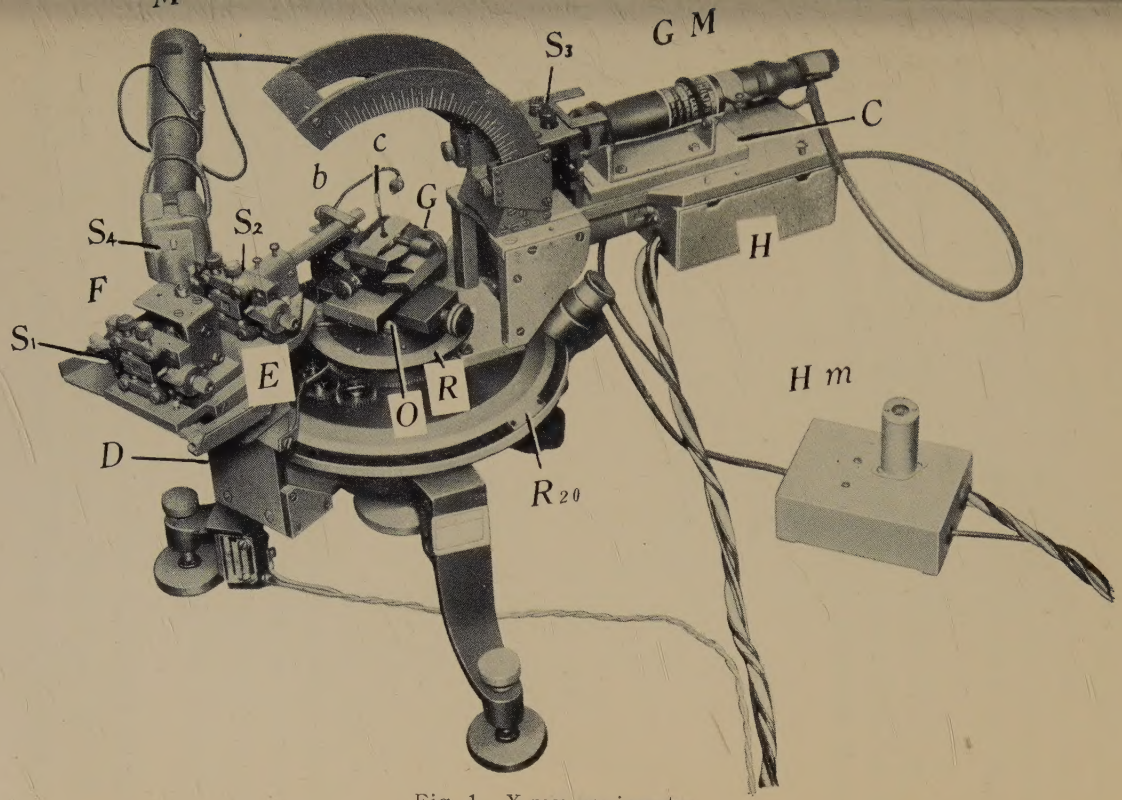

Fig. 1. X-ray goniometer.

E : entrance slit system, C : arm carrying the counter, D : driving mechanism, G : goniometer head, c : specimen crystal, O : shaft, R : circular scale for the goniometer, $R_{2\theta}$: circular scale for reading 2θ angles, S_3 : receiving slit, G.M. : Geiger counter, M : monitoring Geiger counter, S_1 : entrance slit for the monitor, F : Ni foil, H : head amp. for the G.M. counter, Hm : head amp. for the monitoring counter, b : X-ray beam shield and trap.

front of the counter.

The monitoring Geiger counter (M) with its entrance slit (S_4) was mounted on an arm pivoted beneath the nickel foil ($K\beta$ filter for Cu radiation) (F), and was so set as to receive characteristic X-rays ($K\alpha$ lines) diffracted by the foil[1]. This monitoring arrangement ensures excellent stability. If an appropriate correction is made, any change in incident X-ray intensity under usual conditions does not affect the change in measured intensities by more than one percent.

Fig. 2 shows the X-ray optical system of the apparatus. When a monitoring system is employed both the counts from the measuring and the monitoring counter are subject to statistical fluctuations.

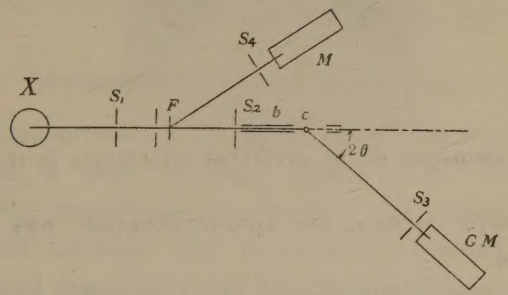

Fig. 2. X-ray optical system.

To minimize the standard deviation of the measurement, it is necessary to receive a strong reflection in the monitoring counter. We used the Cu$K\alpha$ radiation obtained by reflection from the (111) planes of the Ni foil. However, the crystals composing the foil have a high degree of preferred orientation. The texture of the preferred orientation may be examined by taking a Debye-Scherrer photograph (Fig. 3). By rotating the foil in its own plane the strongest beam can be obtained through the slit S_4.

The intensity of the incident beam was made constant by using a sealed off X-ray tube (Norelco Cu target tube) and an autotransformer in the mains supply. To stabilize the primary a.c. sup-

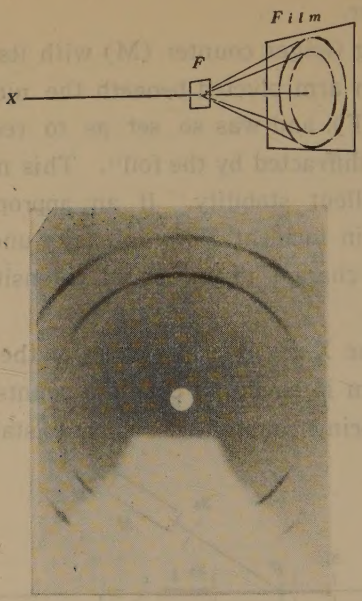

Fig. 3. Examination of the preferred orientation in the Ni foil.

ply for all electric circuits, the auto-transformer was adjusted by manual control.

An argon-chlorine filled Geiger counter (Norelco Type No. 62 019) was used to measure the intensity of X-rays. The electronic counting circuits were essentially the same as those used in the standard Norelco diffractometer. Two sets were constructed, one set was used for monitoring. The counting circuits of the two scalers were controlled simultaneously through an operation switch so that the total number of counts, recorded by both counters in a given interval, can be registered separately. In order to check the effective resolving time experimentally a univibrator circuit (one shot multivibrator) with a known resolving time was temporarily inserted in the first stage of the scaling circuit. Three different values of the resolving time of the scaler was able to be obtained by a selector switch. Fig. 4 shows the schematic diagrams of the scalers.

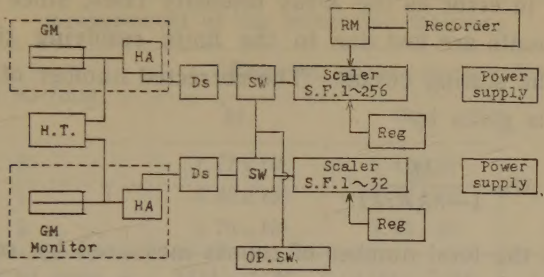

Fig. 4. Schematic diagram of the scalers.

GM : Geiger counter, SW : electronic switching circuit,
H.T. : high tension supply, OP.SW : operation switch,
HA : head amplifier, S.F. : scale factor,
Ds : discriminator, RM : rate meter,
Reg : counting register.

Measurement of the integrated intensity

For the measurement of X-ray intensity diffracted by a given set of planes, a small specimen (about 0.1×0.1×5mm. in size) mounted on the goniometer was dipped in the incident beam, and the integrated intensity was recorded by scanning the crystal through a small angle about the reflecting position.

The driving mechanism scans the peak with constant angular velocity and the counts are totalized on the counting register which is proportional to the whole area under the reflection curve. The velocity was chosen as 1/4 or 1/8 (2θ°/min.). The counter was placed at the reflecting position and the entrance slit was kept sufficiently wide for the whole reflection. A rocking angular range was about 0.6° for the low angle reflections, while it extended to 1.1° for the high angle region, which was determined from the recorded intensity curves for strong reflections. For each reading the following two corrections were made.

Correction for counting loss

The number of counts measured by the Geiger counter will be

increasingly in error as the X-ray intensity rises, since some proportion of counts are lost due to the finite resolving time of the counter or the scaling circuit. The corrected number of counts of a reflection is given by[3]

$$M=\frac{M_0}{1-M_0K\tau/T}, \quad \cdots\cdots(1)$$

where M_0 is the total number of counts measured by rotating the crystal uniformly in a time T through the reflecting position. The form factor K can be calculated from the wave forms of high tension applied to the X-ray tube, (full wave rectified and smoothed by 0.05μF capacitance) and the profile of the reflection. However, in the present study the value K was found experimentally following the method proposed by Cochran[3].

For the determination of the effective resolving time ($K\tau$) a series of measurement was undertaken for a strong reflection with the scaler having the resolving time τ. Let M_1, M_2 and M_3 be the number of total counts recorded with the scaler having the resolving time τ_1, τ_2 and τ_3 respectively, the following relations will hold,

$$\frac{K}{T}(\tau_2-\tau_1)=\frac{1}{M_2}-\frac{1}{M_1}, \quad \frac{K}{T}(\tau_3-\tau_2)=\frac{1}{M_3}-\frac{1}{M_2},$$
$$\frac{K}{T}(\tau_3-\tau_1)=\frac{1}{M_3}-\frac{1}{M_1} \quad \cdots\cdots(2)$$

Since τ_1, τ_2, τ_3 and T are known, one can readily find the value K. Some numerical results obtained for a reflection are shown in Table 1, in which the resolving time of the counting system were chosen* as τ_1=150 sec., τ_2=610 sec. and τ_3=1780 sec., while the crystal rotated in 330 sec. at a speed of 1/8 (°2θ/min.). Three sets of measurements were undertaken with reduced intensity by interposing two nickel foils in the reflected beam. Values of $\frac{1}{M_2}-\frac{1}{M_1}$ etc. are tabulated in Table 1, which lead to K=1.93 (mean). For other

* Determined by the observation on a synchro-oscilloscope.

Table 1. Determination of the form factor for the measurement of the integrated intensity.

No. of Ni foils	Recorded counts for a reflection		
	M_1	M_2	M_3
0	7.77×10^4	6.44×10^4	4.49×10^4
1	5.40×10^4	4.78×10^4	3.60×10^4
2	3.76×10^4	3.38×10^4	2.75×10^4
No. of Ni foils	$1/M_2-1/M_1$	$1/M_3-1/M_2$	$1/M_3-1/M_1$
0	2.66×10^{-6}	6.78×10^{-6}	9.44×10^{-6}
1	2.44×10^{-6}	6.85×10^{-6}	9.28×10^{-6}
2	3.06×10^{-6}	6.72×10^{-6}	9.78×10^{-6}
mean	2.72×10^{-6}	6.78×10^{-6}	9.50×10^{-6}
	$\tau_2-\tau_1$	$\tau_3-\tau_2$	$\tau_3-\tau_1$
	460×10^{-6}	1170×10^{-6}	1630×10^{-6}
K/T	5.91×10^{-3}	5.80×10^{-3}	5.82×10^{-3}
K	1.95	1.91	1.92
K (mean)	1.93		

reflections slightly different K values may be obtained, since each reflection has a different profile. But the error in the value was relatively unimportant unless more than 10^5 counts were recorded for the reflection. (since $\frac{\Delta M}{M}=M\frac{\tau}{T}\Delta K$, taking $M=10^5$, $\tau=150\times16^{-6}$ sec., $T=300$ sec., $\Delta K=0.5$, it gives $\frac{\Delta M}{M}=0.025$). In this connection, Ni foils of known absorption were used to reduce the total counts for the reflection not exceeding about 2×10^4.

Correction for the background

The natural background was measured by recording the total number of counts in a period of 10 min. with the window of the Geiger counter closed.

Table 2. Integrated intensities measured for the $(0kl)$ planes of β-glycine.

hkl	p	$\frac{M_0}{32}$	$\frac{\Delta M}{32}$	$\frac{M}{32}$	$A\times\frac{M}{32}$	t sec	n	T sec	$\frac{N_b}{32}$	$\frac{\Delta M-N_b}{32}$	$\frac{T}{n}\times10^{-1}$	I_0	$\frac{1}{Lp}$	$F_0=\sqrt{\frac{I_0}{Lp}}$	F_0 abs.
001	7	547	8	555	41200	130	966	150	167	41033	1.551	638	0.333	14.55	17.93
011	4	328	3	331	3870	120	974	154	121	3749	1.581	59.3	0.423	5.00	6.17
020	9	300	3	303	77000	90	981	150	67	76933	1.529	1175	0.535	25.01	30.85
021	6	333	3	336	13490	120	762	120	61	13429	1.575	212	0.658	11.80	14.55
002	6	331	3	334	13400	110	852	150	44	13356	1.760	235	0.745	13.21	16.30
012	4	644	12	656	7680	140	912	150	54	7626	1.646	126	0.787	9.94	12.25
022	3	638	14	652	4130	140	929	150	46	4084	1.615	65.9	0.991	8.08	9.96
031	4	328	3	331	3870	100	715	120	30	3840	1.678	64.4	1.005	8.04	9.91
003	0	190	0	190	190	130	1128	180	36	154	1.598	2.45	1.251	1.75	2.16
032	2	368	4	372	1271	110	741	120	29	1242	1.619	20.0	1.318	5.14	6.34
013	3	382	4	386	2440	110	706	120	27	2413	1.699	41.0	1.318	7.35	9.07
040	4	318	3	321	3760	110	701	120	26	3734	1.710	63.9	1.352	9.27	11.46
041	3	281	2	283	1790	110	899	150	26	1764	1.670	29.3	1.448	6.52	8.04
023	0	96	0	96	96	120	910	150	27	69	1.665	1.15	1.500	1.31	1.62
042	0	481	7	488	488	130	924	150	28	460	1.623	7.46	1.718	3.57	4.40
033	0	294	2	296	296	120	1105	180	26	270	1.630	4.39	1.762	2.77	3.42
004	2	300	3	303	1036	120	937	150	25	1011	1.600	16.0	1.854	5.44	6.71
051	1	251	1	252	466	120	738	120	21	455	1.625	7.24	1.890	3.70	4.57
014	0	424	5	429	429	120	892	150	24	405	1.628	6.81	1.890	3.59	4.43
024	0	495	7	502	502	120	894	150	24	478	1.678	8.01	1.970	3.97	4.90
043	0	64	0	64	64	120	734	120	24	40	1.634	0.64	1.980	1.12	1.38
052	0	176	0	176	176	120	912	150	24	152	1.645	2.50	1.982	2.22	2.74
034	0	422	5	427	427	120	952	160	24	403	1.680	6.77	1.992	3.66	4.51

060	0	383	4	387	387	130	879	150	25	362	1.707	6.17	1.978	3.48	4.30
061	0	242	1	243	243	140	1066	180	27	216	1.690	3.65	1.945	2.66	3.28
053	0	242	1	243	243	130	1079	180	27	216	1.670	3.61	1.894	2.62	3.23
005	0	95	0	95	95	80	1201	200	18	77	1.663	1.27	1.870	1.54	1.90
015	0	84	0	84	84	130	1379	210	29	55	1.525	0.84	1.826	1.24	1.53
044	0	157	0	157	157	150	1319	210	32	125	1.593	1.99	1.805	1.89	2.34
062	0									11*	1.63	0.18	1.774	0.54	0.67
025	0									30*	1.69	0.51	1.720	0.94	1.16
035	0	216	1	217	217	150	1063	180	31	186	1.692	3.15	1.420	2.12	2.62
071	0	128	0	128	128	150	1295	210	33	95	1.622	1.55	1.330	1.44	1.78
063	0									5*	1.65	0.09	1.330	0.35	0.43
054	0	325	3	328	328	160	1233	210	34	294	1.701	5.00	1.333	2.58	3.18
072	0	99	0	99	99	180	1592	270	43	56	1.696	0.94	1.013	0.97	1.20
045	0									0.0	—	0.0	0.960	0.0	0.0
006	2	435	6	441	1510	190	1605	270	50	1460	1.682	24.6	0.855	4.58	5.65
016	0									25*	1.682	0.42	0.773	0.57	0.70

p: Number of Ni filters. M_0: Number of counts observed for the integrated intensity. ΔM: Number of counting loss for M_0. M: Corrected number of counts for the integrated intensity. A: Absorption factor for filters ($A=a^p$, where a is the absorption factor for the single Ni filter, $a=1.850$). t: Time during which the integrated intensity was recorded. n: Number of counts recorded by the monitor in a time T. N_b: Number of counts for the background. I_0: Observed integrated intensity (relative scale), calculated by the relation $\frac{A\times M-N_b}{32}\times\frac{T}{n}\times 10^{-2}$. Lp: Lorentz and polarization factors. F_0 abs.: Observed structure factor in absolute scale.

* For these very weak reflections the intensity was measured by integrating the intensity curve recorded on the strip chart.

The X-ray background due to radiation scattered from the air and incoherently from the crystal was measured over the whole angular range by setting the crystal at an angle where no reflected radiation could be recorded.

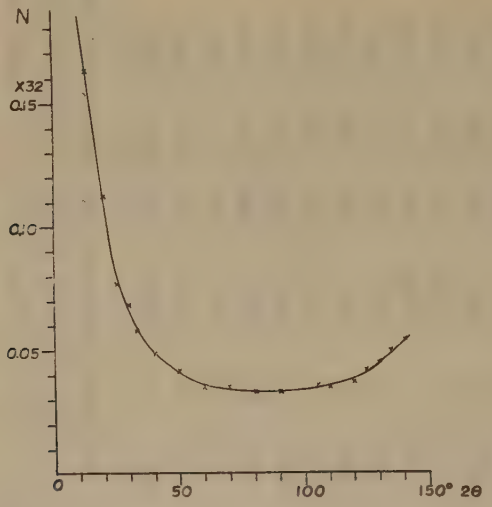

Fig. 5. Background measured for the ($0kl$) layer of β-glycine.

N: The number of counts observed while the monitor records 32 counts.

Contributions from the X-rays of wave length $\lambda/2$ or $\lambda/3$ reflected by the second or third order planes were important in a few reflections; however, the X-ray tube voltage was not so high (30 kV.) and the counter had low sensitivity to these rays (the quantum efficiency for $\lambda/2$ rays drops to one fifth of that for λ), therefore the correction was not made. Fig. 5 shows the background measured for the ($0kl$) layer of β-glycine. These values, including both the natural and X-ray background, were subtracted from the recorded intensity.

The integrated intensities were measured for the ($0kl$) and ($h0l$) planes. The results obtained for ($0kl$) planes are given in Table 2.

Accuracy of the measurement

The statistical standard deviation, estimated from the total number of counts for each reflection, was less than 1% except for the very weak ones. For the weak reflections, for example $F=1.38$, in which the total number of counts of about 8×256 was recorded, the standard deviation averaged about 2.2%. In the case of the very weak reflections, the intensities were measured by integrating the intensity curves recorded on the strip chart. The standard deviations for the measurement increased up to 7% for such planes.

It was confirmed that the intensity of any rflection with medium intensity is reproducible within the allowance of a few percent, while its crystallographically equivalent reflections coincide with it within the allowance of several percent.

Use of a proportional counter and a scintillation counter for the measurement

These two types of counter have rapidly developed in the field of X-ray diffraction work[1) 7)]. They have two distinct features,

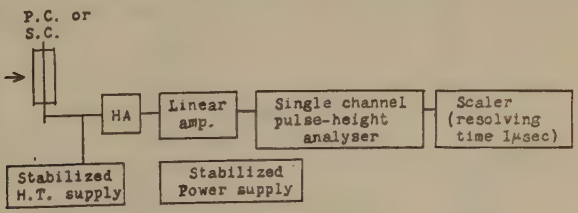

Fig. 6. Schematic diagram of the counting circuits for the proportional and scintillation counter.

P.C.: proportional counter, S.C.: scintillation counter.

The head amplifier (HA), the linear amplifier and the fast scaler circuits are the same as those used in the Norelco scintillation and proportional unit. The single channel pulse-height analyser is of the biased diode type using germanium diodes for discrimination, which was described in the Journal of Scientific Instruments 33, 257 (1956).

namely (1) they have very short resolving time which makes it possible to count at very high rate without counting loss; (2) when the counters are used in conjunction with a pulse-height analyser they have wavelength discriminating properties. In addition, the high quantum efficiency of the scintillation counter is another advantage especially for shorter wavelength radiation such as Mo$K\alpha$. We have tested these counters for the measurement and the results will be briefly described here. The electronic counting system are shown in Fig. 6. The counters used were Norelco type No. 62031 proportional counter[4] (Xe filled, non-quenched, side window) and Norelco type No. 52225 scintillation counter[4] (Tl activated NaI scintillator, DuMont 6292 photomultiplier).

The non-linearity of the Geiger counter due to its long dead

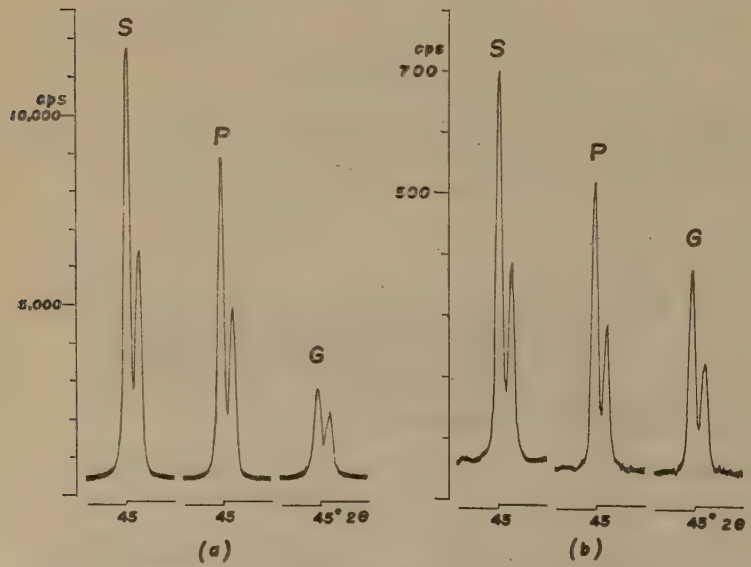

Fig. 7. Intensity curves for a diffraction line (Cu$K\alpha$) from a single crystal specimen recorded by the Geiger (G), proportional (P), and scintillation counter (S), showing the non-linearity of the Geiger counter at high counting rate and the high quantum efficiency of the scintillation counter.

time is a serious disadvantage in the measurement of single crystals, since the strong reflections often exceed the counting rate of about 10^3 cps. and it will generally necessitate a complicated correction for the lost counts as described in the previous section. Such a correction is neither easy nor accurate especially for the measurement of integrated intensities. Moreover, for intensities exceeding about 10^3 cps. corrections are no longer possible and it will be necessary to reduce the intensities by interposing absorption foils in the X-ray path. The proportional and the scintillation counters have much better linearity, non-linearity will occur only at 10^4 cps. or even higher (the amount of counting loss is less than 1.7% at 10^4 cps. if the resolving time is 1μ sec.) and the corrections are not necessary in most cases. Fig. 7 shows intensity curves for a strong reflection recorded by these counters.

The possibility of discriminating between different wavelength radiations may serve to eliminate the background pulses which consist chiefly of the following contributions: radiation of a continuous spectrum scattered by the specimen, fluorescent X-ray radiation excited in the specimen, cosmic rays (the background due to radiation having the same wavelength as that of the characteristic X-rays cannot be eliminated). Fig. 8 shows the pulse-height distribu-

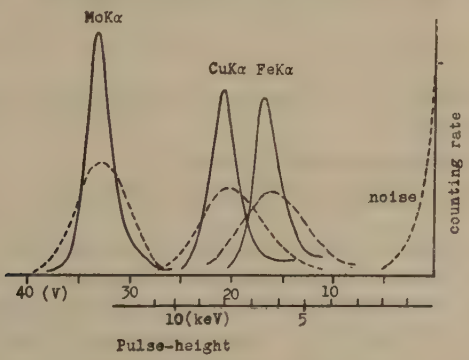

Fig. 8. Pulse-height distribution observed by the proportional (full lines) and scintillation counter (broken lines).

tion curves for some characteristic radiations observed by both the proportional and scintillation counter. It will be seen that the distribution observed by the latter is considerably broader than the former but the spread is small enough to reject the second harmonics of the radiation. In this connection, the scintillation counter used in conjunction with a pulse-height discriminator will in most cases be preferred for the measurement owing to its much higher quantum efficiency. However, when the background contains fluorescent radiation the proportional counter with pulse-height discrimination

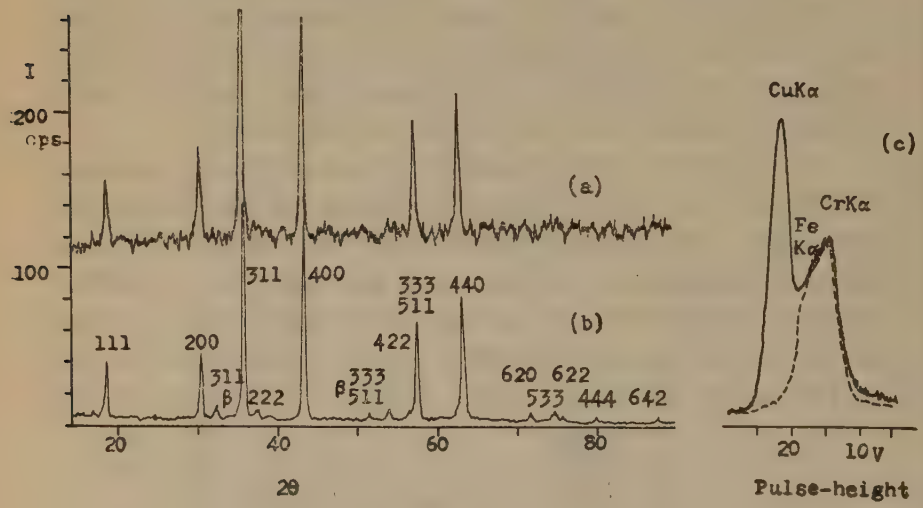

Fig. 9. Reduction of fluorescent background with pulse-height discrimination.

Specimen: chromite powder [$FeCr_2O_4$].
Cu radiation Ni filtered, 30kV. 15mA., scale factor 4, time const. 4 sec..

(a): proportional counter without pulse-height analyser.
(b): proportional counter with pulse-height analyser.
(c): pulse-height distribution curves measured at the background (dotted line) and at the peak (full line), which show that the background pulses are generated mainly by fluorescent X-rays of the excited specimen. These background pulses are discriminated by the pulse-height analyser as shown in (b).

may be more effective in the reduction of the background (Fig. 9).

Acknowledgement

The writer wishes to express his sincere thanks to Prof. T. Ito, Dr. R. Sadanaga and Dr. T. Takeuchi for their guidance. Thanks are also due to Dr. H. Inuzuka and Dr. M. Nakahira for their valuable advice. This study has been supported in part by a Grant for the Scientific Research from the Ministry of Education.

References

1) Arndt, U.W., W.A Coates and D.P. Riley: Proc. Phys. Soc., B66, 1009 (1953).
2) Bommel, A.J. and J.M. Bijvoet: Acta Cryst., 11, 61 (1958).
3) Cochran, W.: Acta Cryst., 3, 368 (1950).
4) Dowling, P.H. et al.: Philips Tech. Rev., 18, 262 (1956, 7).
5) Evans, H.T.: Rev. Sci. Instrum., 24, 156 (1953).
6) Lonsdale, K.: Acta Cryst., 1, 12 (1948).
7) Peiser, H.S. et al.: "X-ray Diffraction by Polycrystalline Materials" The Institute of Physics, London, 201 (1955).
8) Pringle, G.E.: Acta Cryst., 7, 716 (1954).
9) Ramachandran, G.N. and W.A. Wooster: Acta Cryst., 4, 335 (1951).
10) Wooster, W.A., G.N. Ramachandran and A. Lang: J. Sci. Instrum., 25, 405 (1948).
11) Zachariasen, W.H.: Acta Cryst., 7, 305 (1954).

Manuscript received July 18, 1958.

Mineralogical Journal, Vol. 2, No. 5, 298-310, Dec., 1958

ALUMINIAN SERPENTINE AND ASSOCIATED CHLORITE FROM USAGIYAMA, FUKUOKA PREFECTURE, JAPAN

Haruo Shirozu

Department of Geology, Faculty of Science, Kyushu University

Abstract

Serpentine-like materials associated with clinozoisite rock in serpentinite were investigated with chemical, X-ray and thermal methods, and it was revealed that the materials are mechanical mixtures of two polymorphic minerals, namely, aluminian serpentine and chlorite which are chemically similar (intermediate between serpentine and clinochlore) and of low crystallinity. The aluminian serpentine has an ortho-hexagonal cell and belongs to the aluminian serpentine series recently synthesized. The closely associated chlorite may have also an ortho-cell.

Introduction

In the course of his study on chlorite and serpentine minerals in Japan, the writer found that some serpentine-like materials associated with clinozoisite rock in serpentinite have unusual properties: the chemical compositions (Al_2O_3 7.9~11.4%) are intermediate between those of serpentine and ordinary magnesium chlorite or Al-poor chlorite, the X-ray powder patterns are of ortho-hexagonal features with weak (001), 14Å and (003) reflections and with strong (002) and (004) reflections, and the differential thermal curves are those of mixtures of two distinct minerals. From these properties, the materials seem apparently to be the mixtures of serpentine and magnesium chlorite which is rich in aluminum (clinochlore). Detailed X-ray data, however, are not consistent with this interpretation, and suggest that the materials are the mixtures of magnesium chlorite which is poor in aluminum and aluminian serpentine.

This aluminian serpentine, being low in aluminum content as well as in crystallinity may belong to the aluminian serpentine series recently synthesized [7)8)11)]. The closely associated chlorite is also of low crystallinity and in some details different from the ordinary chlorites.

Mode of occurrence and microscopic observation

To the east of Fukuoka City, Kyushu Island, there are several serpentinite bodies within the area of low-grade crystalline schists and Paleozoic rocks which are surrounded by granite masses. The reference materials are found associated with clinozoisite rocks in one of the serpentinite bodies, which contains small ore deposits of chromite, at Usagiyama, Daibu Village, Kaho County, Fukuoka Prefecture. The clinozoisite rock occurs as rounded small compact masses (about 5 to 50 cm. in diameter) along a sheared zone of serpentinite, and consists of clinozoisite, calcite and a small amount of chlorite.

The materials in question are found either as thin shells of the clinozoisite rocks or as veinlets within them, up to 5 mm. in thickness, apparently of secondary origin. They are pale olive-green in colour, translucent and resinous in luster, having some resemblance to a kind of serpentine. Under the microscope, they form subparallel aggregates of colourless fine scales with optically positive elongation, and look like as if they were composed of a monomineralic serpentine. The refractive indices vary in portions from 1.55 to 1.565. The double refraction is low.

The chlorite in the clinozoisite rock, forming spherulitic aggregates among clinozoisite crystals, is well crystallized ordinary chlorite (leuchtenbergite-sheridanite) of which the elongation is negative and the X-ray powder pattern is of 14Å-monoclinic type[9)], thus being quite distinct from the materials in question.

Reference specimens

The specimens were found to vary in X-ray and thermal proper-

ties, although they show no noticeable difference in both macroscopic and microscopic features. Specimen No. 1 however bears a little lower refractive indices (1.55~1.56) than the other two (1.555~1.565). The selected three type specimens (Nos. 1~3) are most representative in both X-ray and thermal properties, and among them No. 2 type is predominent. Before experiments, every specimen was treated with cold dilute hydrochloric acid to disolve away a small quantity of calcite in it.

Specific gravity and chemical composition

The specific gravites measured by picnometer and the chemical analyses for the type specimens are given in Table 1. It shows that the chemical compositions of specimens Nos. 2 and 3 are quite similar, but specimen No. 1 has less Al_2O_3 and more SiO_2 and $H_2O(-)$. These chemical compositions are intermediate between serpentine and ordinary chlorite (clinochlore) or those of Al-poor chlorite. The interpretation for chemical data will be presented in the last section.

Table 1. Specific gravities and chemical compositions of the mixtures of chlorite and aluminian serpentine from Usagiyama.

	Specimen No. 1	Specimen No. 2	Specimen No. 3
Sp. Gr.	2.47	2.55	—
SiO_2	38.63%	36.60%	36.77%
Al_2O_3	7.90	11.33	11.42
Fe_2O_3	0.15	0.26	0.22
FeO	1.54	1.54	1.84
MnO	0.06	0.05	0.05
MgO	35.88	36.35	36.36
CaO	0.42	0.14	0.10
H_2O^+	13.01	13.51	13.36
H_2O^-	2.50	0.89	0.64
	100.09%	100.67%	100.76%

Analyst: H. Shirozu.

X-ray powder studies

X-ray powder patterns were taken by a Norelco X-ray diffractometer as well as by a conventional powder camera. The smoothed traces of the diffractometer patterns for specimens Nos. 1~3 are shown in Fig. 1. The reflections are generally more diffuse than those of usual serpentine or chlorite, and the lines of No. 1 are broader and weaker than those of Nos. 2 and 3. Although the angles of corresponding reflections of the specimens are in good accordance with each other, their intensities, particularly of basal reflections,

Fig. 1. Smoothed traces of diffractometer patterns of the mixtures of aluminian serpentine and chlorite from Usagiyama (1)~(3), and the purified aluminian serpentine (4).
(1) specimen No. 1, (2) specimen No. 2, (3) specimen No. 3, Filtered Cu radiation.

are distinct from each other.

The diffraction data for No. 2 obtained by the diffractometer are given in Table 2 together with those by the conventional camera, which are less effected by the preferred orientation than the former. No long spacing (up to 40Å) is recorded. The cell of 14Å was not expanded by ethylen-glycol treatment.

These powder patterns show ortho-hexagonal features, e. g., the lines for No. 2 can be indexed in terms of a cell with $a=b/\sqrt{3}$, $b=9.21$Å, $c=14.46$Å, $\beta=90°$, as listed in Table 2. The lines indexed as (020), (200) and (240) appear to be the terminations of *hk* diffraction bands. These patterns bear some resemblances to ortho-hexagonal Fe-rich chlorites[9], and also to amesite[1] or ortho-serpentines[10)12)] except for the weak (001) and (003) reflections. But there are few reference X-ray or thermal data which indicate the existence of serpentine-chlorite mixed-layer structure.

Taking chemical and thermal data into consideration as well, the specimens are interpreted as mechanical mixtures of serpentine and chlorite in varying proportions; No. 1 is poor in chlorite, while No. 3 is rather rich.

It is known that the basal spacings of serpentine and chlorite minerals vary equally according to the variations in bonding forces between the tetrahedral and octahedral layers, that is, to the degree of the substitution of Al^{3+} ions for cations in both layers[2)3)4)5)9)]. Therefore, if the materials were the mixtures of Al-free serpentine and Al-rich chlorite, then the difference of the corresponding basal spacings of the two phases should be recognized; it should be in the way either that the (002) and (004) reflections separate into two peaks, or that d(001) spacings calculated from (002) and (004) reflection angles show a little larger values than those from (001) and (003). Neither of them is the case with the specimens from Usagiyama, that is: (1) the (002) and (004) reflections, even under a slow scanning speed, give single and symmetrical curves, and (2) the d(001) spacings calculated from the (001)~(004) reflection

Table 2. X-ray powder data for specimen No. 2.

hkl	$d_{calc.}$	1		2	
		d(Å)	I	d(Å)	I
001	14.46	14.57	13	14.3	3
002	7.23	7.242	100	7.2	10
003	4.820	4.823	12	4.85	2
020	4.605	4.575	35	4.59	6
022	3.883	3.883	5		
004	3.615	3.615	70	3.62	8
005	2.892	2.873	7	2.88	½
024	2.843				
200	2.658	2.657	8	2.62	2
201	2.614	2.610	12		
202	2.495	2.495	50	2.49	9
025	2.448	2.450	17		
203	2.328	2.330	5	2.33	1
204	2.142	2.139	12	2.14	3
205	1.957	1.957	7	1.96	2
206	1.785	1.787	6	1.79	2
240	1.740	1.737	7	1.74	2
207	1.631	1.630	3	1.63	½
060	1.535	1.536	30	1.54	7
062	1.502	1.502	14	1.50	4
0010	1.446	1.445	5	1.45	½
064	1.413	1.412	4	1.41	1
209	1.375	1.373	3	1.38	½
401	1.324	1.326	5	1.33	1
402	1.307	1.308	12	1.31	3
403	1.281			1.275	1
2010	1.270				
405	1.208			1.207	½
0012	1.205				
406	1.164			1.166	1
408	1.071			1.072	½
0610	1.053			1.054	1

(1) Data by diffractometer. Filtered Cu radiation.
(2) Data by conventional powder camera. Filtered Cu radiation, camera radius 45 mm.

angles which are calibrated by using an internal standard show that the (00l) reflections form a rational series (Table 3).

Table 3. X-ray data for the basal spacings (in Å).

l	Specimen No. 1		Specimen No. 2		Specimen No. 3	
	d(00l)	d(001)	d(00l)	d(001)	d(00l)	d(001)
1			14.57	14.57	14.43	14.43
2			7.241	14.48	7.242	14.48
3			4.823	14.47	4.827	14.48
4	3.620	14.48	3.615	14.46	3.615	14.46

The d(00l) values were calibrated respectively by adopting the (001)~(004) reflections of the well crystallized chlorite (leuchtenbergite) from Muramatsu[6][9] with d(001)=14.182Å as an internal standard. Cu$K\alpha$.

Moreover, these d(001) values are intermediate between those of chlorite and Al-free serpentine (Table 4).

These X-ray data suggest that the two phases in question may have a similar chemical composition; the one being aluminian serpentine and the other, chlorite poor in aluminum. The optical properties presented above, although apparently monomineralic, also support this interpretation.

For the determination of more detailed properties of the two constituent minerals, specimen No. 2 was purified by removing the associated chlorite by acid-treatment after heating up to 550°C. (the method of Brindley and others[1]). The X-ray pattern of this purified aluminian serpentine is illustrated as trace (4) in Fig. 1, which shows the coexistence of a little amount of silica gel. Its (20l) reflections are very similar to those of the untreated specimen No. 2 which give (20l) lines with odd l, showing that the aluminian serpentine has a two-layered structural base. But the relative weakness of intensities of (20l) lines with odd l compared with those with even l suggests that an one-layered cell is mixed.

Because of impurities, the detailed X-ray properties of the associated chlorite could not be investigated. However, since no distinct monoclinic reflections of chlorite was detected (Fig. 1), this chlorite may also have an ortho-hexagonal cell.

Differential thermal analyses

The d.t.a. curves of the specimens are shown in Fig. 2. The curve of No. 1 is apparently of monomineralic nature, while those of Nos. 2 and 3 are clearly of mixtures. The curve of the purified aluminian serpentine obtained from No. 2 is denoted by (4) in Fig. 2.

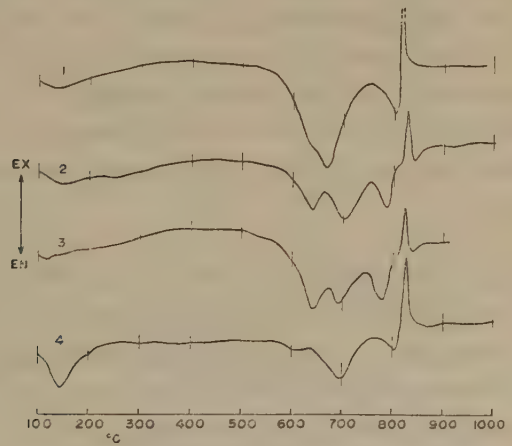

Fig. 2. Differential thermal analysis curves of the mixtures of aluminian serpentine and chlorite (1)~(3), and the purified aluminian serpentine (4).
(1) specimen No. 1, (2) specimen No. 2, (3) specimen No. 3.

The two curves, (2) and (3) are essentially identical with three endothermic peaks between 600°C. and 800°C., among which the second peak is more distinct with (2) than with (3). The first and third endothermic peaks are considered to be due to chlorite phase and the second one, to serpentine phase, according to the X-ray data for thermal changes which will be presented in the next section of

this paper.

The curve (1) is fairly different from the curves (2) and (3), and rather resembles to the curve (4), suggesting that among the three specimens No. 1 is the lowest in chlorite content. The temperature of endothermic reaction, however, is lower with (1) than with (4). This is infered to be due to its lower crystallinity as suggested also by the X-ray and other properties. The very distinguished endothermic peak may refer to the overlapping effect of serpentine and chlorite phases.

The endothermic peak at 140°C. of curve (4) is perhaps due to the adsorbed water of silica gel which has been formed by the heat- and acid-treatment, and the endotherm at 610°C. may be due to the residual chlorite which could not be recognized on the X-ray pattern.

The temperatures of endotherms and exotherms of all the three specimens are somewhat lower than the corresponding temperatures of ordinary serpentine and chlorite, indicating the low crystallinity of the specimens.

Effects of heating on the X-ray powder pattern

The effects of heating on the powder pattern were examined. Specimen No. 2 was heated in air for one hour at every 50° from 500° to 800°C., and powder patterns were taken after cooling. The results (Fig. 3) indicate the following sequence of events; (1) the first dehydration of chlorite (550°～600°C.), (2) decomposition of aluminian serpentine (600°～700°C.), (3) the second dehydration and decomposition of chlorite (650°～700°C.), (4) the beginning of crystallization of forsterite (700°C.), and (5) the beginning of crystallization of enstatite (800°C.). A noteworthy event at 750°C. is the disappearance of basal reflection, whereas weak prismatic *hk*0 reflections remain (indicated by an arrow in Fig. 3).

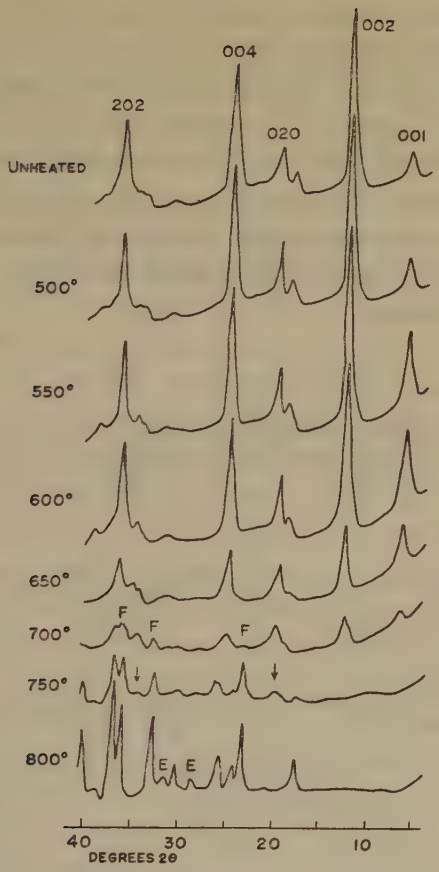

Fig. 3. Smoothed traces of diffractometer patterns for the heated specimen No. 2. Filtered Cu radiation.

F: forsterite. E: enstatite.

Summary and discussion

From the above experiments, the specimens in question are infered to be the mechanical mixtures of aluminian serpentine and chlorite in varying proportions. The important properties of the two mineral phases are as follows.

Their crystallinity, in particular of specimen No. 1, is fairly lower than the ordinary serpentine and chlorite. The cell of aluminian serpentine is infered to be two-layered ortho-hexagonal, while that of chlorite one-layered ortho-hexagonal. Accepting these cell structures, the cell dimensions of the two minerals are almost identical as shown in Table 4. Their chemical compositions as interpreted from X-ray data, are also similar. Therefore, they are polymorphous. Their structural formulae evaluated on the basis of O+(OH)=18 atoms are as follows:

Specimen No. 1

$$\underbrace{(Ca_{.04}Mg_{5.06}Fe^{2+}_{.13}Fe^{3+}_{.01}Al_{.54})}_{5.78\text{ atoms}}\quad\underbrace{(Al_{.34}Si_{3.66})}_{4\text{ atoms}}\quad\underbrace{O_{9.78}(OH)_{8.22}}_{18\text{ atoms}}$$

Specimen No. 2

$$\underbrace{(Ca_{.01}Mg_{5.02}Fe^{2+}_{.12}Fe^{3+}_{.02}Al_{.63})}_{5.80\text{ atoms}}\quad\underbrace{(Al_{.61}Si_{3.39})}_{4\text{ atoms}}\quad\underbrace{O_{9.65}(OH)_{8.35}}_{18\text{ atoms}}$$

Table 4. Cell dimensions of some serpentine and chlorite minerals.

	1	2	3	4	5	6
a	5.31Å	$b/\sqrt{3}$=5.32 Å	$b/\sqrt{3}$=5.32 Å	—	$b/\sqrt{3}$	$b/\sqrt{3}$
b	9.20	9.21	9.21	—	9.20~9.24 Å	9.17kX
c	14.62	14.48	14.46	d(001)= 7.06~7.17 Å	$c\sin\beta$= 14.1~14.3	13.98
β	90°	90°	90°			90°

(1) Ortho-chrysotile[19].
(2) Aluminian serpentine and chlorite of specimen No. 1 from Usagiyama.
(3) Aluminian serpentine and chlorite of specimens Nos. 2 and 3 from Usagiyama.
(4) Synthetic aluminian serpentines.[7][8]
(5) Mg-chlorites.[9]
(6) Amesite from Chester.[1]

Specimen No. 3

$$\underbrace{(Ca_{.01}Mg_{5.01}Fe^{2+}_{.17}Fe^{3+}_{.02}Al_{.85})}_{5.84\text{ atoms}}\quad\underbrace{(Al_{.60}Si_{3.40})}_{4\text{ atoms}}\quad\underbrace{(O_{9.75}(OH)_{8.25}}_{18\text{ atoms}}$$

It is well known that there is a gap in chemical composition between serpentine and chlorite. The specimens above described fall near or within the area of the gap, suggesting some bearing on their genesis. And, although neither serpentine nor chlorite mineral identical with them is ever known, some similar minerals have been reported as commented below.

Chester amesite[1], which contains much alumina, has a two-layered ortho-hexagonal cell and is associated with chlorite as closely as the Usagiyama aluminian serpentine. Serpentine minerals with ortho-hexagonal cells are known as ortho-chrysotile (two-layered) or lizardite (one-layered)[10]. The X-ray data for the synthetic aluminian serpentine obtained by D.M. Roy and R. Roy[7] seem to bear an ortho-hexagonal cell, and those by H.S. Yoder[11] seem likely to be a polymorphic mixture, one of which possibly bears an ortho-cell.

The chemical composition of the chlorite under investigation is similar to that of pennine, but its cell is different from that of 14Å-monoclinic pennine, and is probably 14Å-ortho-hexagonal. Since the chlorites with 14Å-ortho-hexagonal cells are common among iron-rich chlorites in Japan[9], the chlorite in question may be correlated to the Mg-rich member of the group. In some respects, however, it somewhat resembles "pseudo-chlorite", giving room for further research.

The genesis of the minerals described is an interesting problem. They occur as mixture and apparently of secondary origin (segregation vein) in contrast with the well crystallized serpentines and chlorites of the country rocks. This mode of occurrence suggests their low-temperature environment of formation which may have defined their characteristic chemical and crystallographic properties. There are some possibilities that these mixed materials were at first formed

as aluminian serpentine, essentially an unstable phase, and then partially separated into the two phases. Various properties as revealed by the present writer and the data of synthetic experiments[5)7)8)11)] as well as the mode of occurrence seem to favour this consideration. The further discussion on these genetical problems, in relation to the associated other minerals will be given in the near future.

Acknowledgements

I wish to acknowledge to Professor T. Yoshimura of Kyushu University for his valuable suggestions and advise. Thanks are due to Messrs K. Muta, H. Momoi, M. Yoshinaga and K. Motoyama of Kyushu University for their help and discussions. I am also greatly indebted to Professor R.E. Grim of University of Illinois who critically read this manuscript.

References

1) Brindley, G.W., B.M. Oughton and R.F. Youell: Acta Cryst., **4**, 552 (1951).
2) Brindley, G.W. and F.H. Gillery: Am. Min., **41**, 169 (1956).
3) Hey, M.H.: Min. Mag., **30**, 277 (1954).
4) Mikheev, V.I.: Zapiski Vsesoyuz. Min. Obshchestra, **82**, 214 (1953). [Ref. Chem. Abs., **48**, (4), 1903]
5) Nelson, B.W. and R.Roy: Proc. Second National Conference on Clays and Clay Minerals, 335 (1954).
6) Okamoto, Y. and H. Shirozu: Mem. Fac. Sci. Kyushu Univ., Ser. D, **5**, 185 (1957).
7) Roy, D.M. and R. Roy: Am. Min., **39**, 957 (1954).
8) Roy, D.M. and R. Roy: Am. Min., **40**, 147 (1955).
9) Shirozu, H.: Miner. Jour., **2**, 209 (1958).
10) Whittaker, E.J.W. and J. Zussman: Min. Mag., **31**, 107 (1956).
11) Yoder, H.S.: Am. J. Sci., Bowen Volume, 569 (1952).
12) Zussman, J., G.W. Brindley and J.J. Comer: Am. Min., **42**, 133 (1957).

Manuscript received June 25, 1958.

Mineralogical Journal, Vol. 2, No. 5, pp. 311-332, Dec., 1958

A DETAILED INVESTIGATION OF THE STRUCTURE OF HEXAGONAL $BaAl_2Si_2O_8$ WITH REFERENCE TO ITS α-β INVERSION

Yoshio Takéuchi

Mineralogical Institute, University of Tokyo

Abstract

The re-examination of the crystal structure of α-hexagonal $BaAl_2Si_2O_8$ has revealed that the true symmetry of the crystal is lower than hexagonal—possibly, orthorhombic with a body centered lattice of dimensions: $a=5.293$, $b=9.168$ and $c=7.79\times2$ Å, and the crystals invariably occur in a trilling form made up by three orthorhombic individuals, simulating a hexagonal symmetry. Since it was not possible to distinguish the reflexions of each individual crystal from those of the others, the avarage structure with the hexagonal lattice, $a=5.293$, $c=7.790$ Å, was investigated by the use of three-dimensional Fourier methods. The structure thus determined shows that the hexagonal $(Al_2Si_2)O_8$ sheets, which were reported in the previous work, are not exactly as such but trigonal owing to a slight deformation. In the structure, the barium atoms are coordinated by six oxygen atoms with the distance of 2.89 Å, and the $Si_{\frac{1}{2}}Al_{\frac{1}{2}}$-O distances vary from 1.65 Å to 1.67 Å, giving the mean value of 1.66_5 Å.

A closer examination of the structure of the β-form on the basis of X-ray powder diffraction patterns and oscillation photographs taken at temperatures above 300°C. appears to disclose that the structure of the form is exactly hexagonal with $a=5.313$ Å, $c=7.805$ Å (at about 450°C.). The space group is D^1_{6h} and there is one formula unit per cell. Thus the $(Al_2Si_2)O_8$ sheets in this form display a regular hexagonal symmetry, and the α-β inversion would be adequately explained as due to the change in configurations of the $(Al_2Si_2)O_8$ sheets from hexagonal to trigonal and vice versa.

Introduction

The structure of α-hexagonal $BaAl_2Si_2O_8$ as found by trial-and-error method[8] was believed to be essentially correct, since with the

structure a satisfactory agreement between the calculated and the observed structure factors was obtained. Nevertheless, because of the presence of heavy Ba atoms, the parameters of the other atoms, especially those of oxygen atoms, are considered as liable to large errors. For instance, the $Al_{\frac{1}{2}}Si_{\frac{1}{2}}$-O distance and the Ba–O distance found in the earlier work as 1.57 Å and 3.05 Å respectively, reveal considerable deviations from the empirical values for these distances. It is also difficult, with the structure, to find any reasonable explanation of the α–β inversion which takes place at 295±5° C.[4]. The refinement of the structure was, accordingly, carried out.

Nomenclature

At the time when the hexagonal crystal with chemical composition of $BaAl_2Si_2O_8$ was artificially prepared by Yoshiki, it was called "α-celsian" after Dittler and Lasch. It had already been established, however, that α- and β- modifications exist in the α-celsian itself[17]. The name was, therefore, considered to be not suitable and later changed to "hexacelsian". On the other hand, a similar substance was also synthesized by Davis and Tuttle and has described as "hexagonal $BaAl_2Si_2O_8$"[4].

Under these circumstances, to avoid unnecessary confusion, the term "hexagonal $BaAl_2Si_2O_8$" is tentatively adopted in the present paper. Thus, β- "hexagonal $BaAl_2Si_2O_8$", for instance, is equivalent to β- "hexacelsian" and to β- "α-celsian".

However, in view of the fact that the true symmetry of the α- form has been found to be lower than hexagonal as described in the present paper, it might invite another confusion to call the substance by the above term and further change of nomenclature may be desirable.

Lattice constants and symmetry

The lattice constants found in the previous work[8] were; a=5.25 Å, c=7.84 Å and space group was D^1_{6h}—C6/mmm. However, re-

examination of the oscillation photographs around the a- and the c-axis (taken with nickel-filtered CuK radiation, λ=1.5418 Å) showed a few weak extra reflexions in between the layer lines, indicating

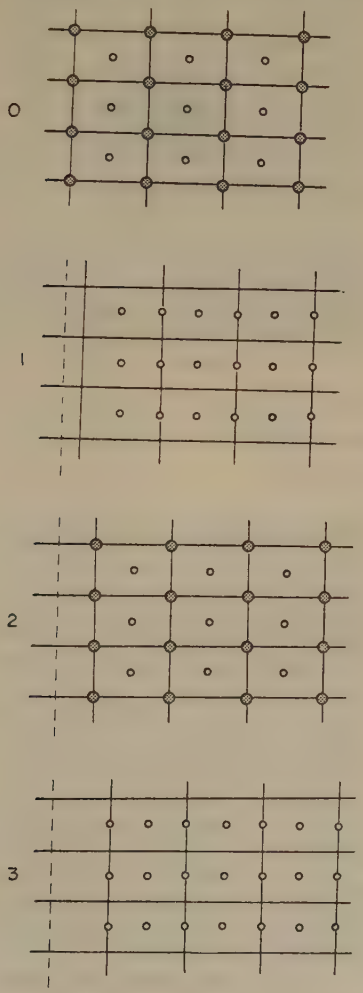

Fig. 1. The reciprocal-lattice nets showing zero (0), first (1)-, second (2)- and third (3)- layer Weissenberg photographs of α-hexagonal $BaAl_2Si_2O_8$. The open circles indicate the positions of weak extra reflexions.

doubling of the *c*- as well as *a*-length. In Weissenberg photographs of even levels around the *a*-axis, the weak extra reflexions are located at the centers of the reciprocal reticular meshes and in those of odd levels, they appear as shown in Fig. 1. The Laue photographs taken perpendicular to (0001) showed the perfect D_{6h} symmetry (Plate I, Fig. 2). And it was established by the detailed examination of the precession photographs that the intensity distribution of the diffraction pattern including the weak reflexions is strictly conformable with hexagonal symmetry (Plates II, III, Fig. 3).

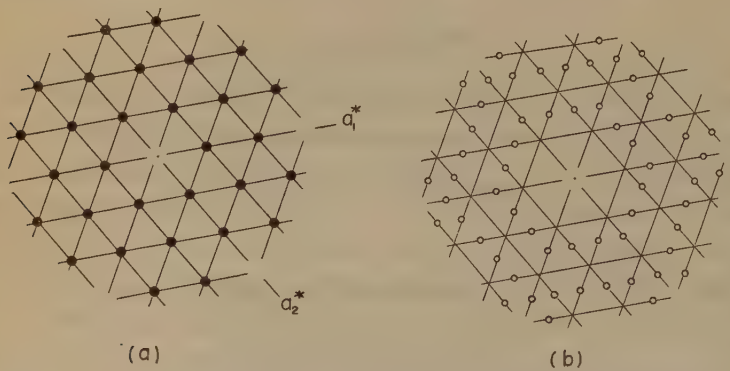

Fig. 4. The reciprocal-lattice nets showing (*hk*0) net plane (a) and (*hk*l) net plane (b) of Buerger precession photographs.

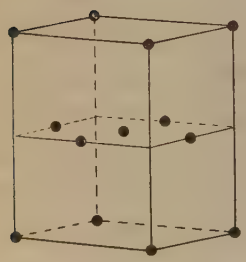

Fig. 5. Reciprocal lattice unit derived from X-ray data.

These X-ray data give the reciprocal lattice unit as shown in Fig. 5, which, inspite of the hexagonal nature, corresponds neither to the hexagonal Bravais lattice nor to the rhombohedral one. It is, therefore, to be interpreted that the lattice is a composite of those with lower symmetry and it may best be explained as the result of trilling of body-centered orthorhombic lattices with

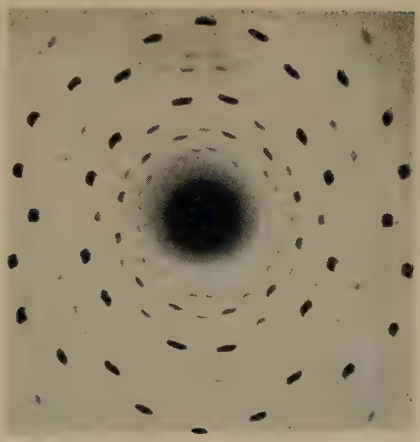

(a)

Fig. 2. (a) Laue photograph of α-hexagonal $BaAl_2Si_2O_8$ taken with the X-ray beam normal to the basal plane.

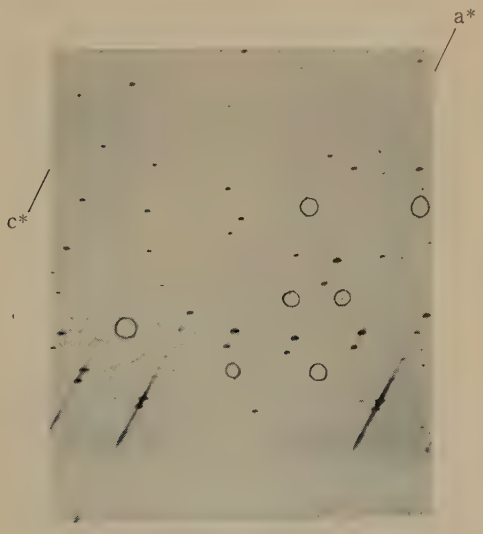

(b)

Fig. 2. (b) Part of zero-level Weissenberg photographs around the a-axis. Weak extra spots are marked by circles.

(a)

Fig. 3. Buerger precession photographs of α-hexagonal $BaAl_2Si_2O_8$.
(a) ($hk0$) net plane. Nickel-filtered CuK radiation, 35kV., 15mA., one hour.

(b)

Fig. 3. (b) ($hk1$) net plane showing weak extra reflexions. Unfiltered CuK radiation, 35kV., 15mA., 12 hrs.

(c)

Fig. 3. (c) (*hk*2) net plane. Unfiltered Cu*K* radiation, 35kV., 15mA., one hour.

the constants; $a_0=a$, $b_0=\sqrt{3}\,a$ and $c_0=2c$. In fact, the trilling of these orthorhombic cells around their common c-axis by angular rotations of 120° and 240° will give rise to an arrangement of reciprocal lattice points corresponding to the experimental data (Fig. 6). It, therefore, seems probable to conclude that α-hexagonal $BaAl_2Si_2O_8$ has a body centered orthorhombic cell and its hexagonal appearence is merely the results of their trilling.

The lattice constants of the hexagonal pseudo-cell and those of the orthorhombic cell are compared as follows:

hexagonal pseudo-cell	orthorhombic cell
$a=5.293\pm0.005$ Å	$a_0=a=5.293\pm0.005$ Å
$c=7.790\pm0.005$	$b_0=\sqrt{3}\,a=9.168\pm0.005$
	$c_0=2c=7.790\times2$
$V=378.0$ Å^3	$V=378.0\times4$ Å^3
$Z=1$	$Z=4$

The above cell dimensions were obtained from powder data (which will be given in the following paragraph) and slightly different

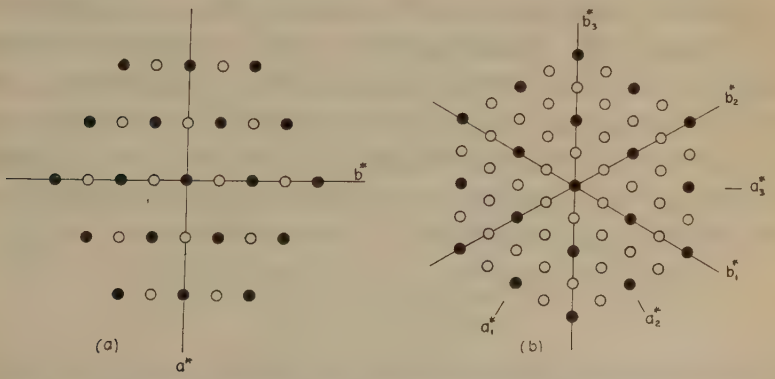

Fig. 6. (a) Zero and first level of the reciprocal lattice of a body-centered orthorhombic lattice from c-axis rotation.
(b) Distribution of the reciprocal lattice points in a trilling form made up of the three orthorhombic individuals.
●.....zero level. ○.....first level.

from those previously reported. The re-calculated density 3.29$_6$ g.cm^{-3} was in good agreement with the observed value 3.29 g.cm^{-3}.

Intensity Measurements

Intensities, except those of *hk*0 reflexions, were recorded in Weissenberg films with the multiple film technique and were estimated visually. However, because of the heighly perfect cleavage like micas, it was not possible to prepare specimens with ideal cross sections so as to minimize the effect of absorption. A special consideration of absorption correction is, thus, required for the strongly absorbing crystal like this barium compound (μ=500 cm^{-1}).

1. Absorption corrections for reflexions from thin crystal plates

In Weissenberg photographs taken by rotating a thin crystal plate around an axis parallel to the plate, there occur linear loci of high absorption in the photograph[15]. The situation is similar in precession photographs[16]. For this particular case, therefore, precession photography does not help to reduce the absorption effect.

Since the cross section of the specimen could be approximated to a rectangle with dimensions, 0.013×0.0027 cm., Albrecht's method modified by the use of Howell's loci of points with constant path length[9] was applied. The transmission factor, T_{h0l}, which is the ratio between the observed intensity, I'_{h0l}, and the ideal intensity, I_{h0l}, is expressed in terms of p, the number of parallelograms in a band for which the path length is approximately x;

$$T_{h0l}=\Sigma p \exp\left[-\mu x\right]/\Sigma p .$$

For a given ω, the angle between the direction of the X-ray beam and the normal of the crystal plate, T_{h0l} was evaluated for each direction of Υ=180°, 160°,——, 20°, 0°, at each of 0°, 10°, 20°,——, 90° for ω. A chart showing equal-T_{h0l} curves was thus prepared for the Weissenberg films and is shown in Fig. 7.

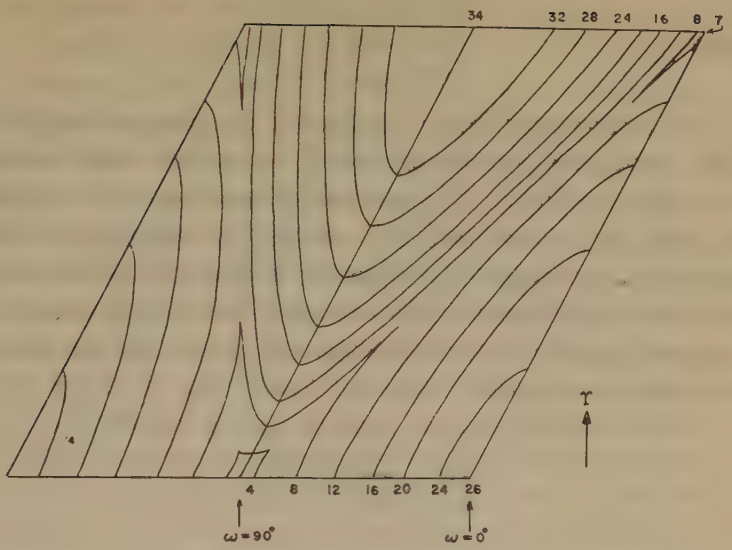

Fig. 7. Equal-transmission factor curves in the Weissenberg films, $\mu=500\,\mathrm{cm}^{-1}$, dimensions of cross section: 0.013×0.0027 cm.

2. Corrections for spot size

For platy crystals, the effect of spot size on the accurate intensity measurement should also be considered. The breadth of a spot, in a Weissenberg photograph, is minimum along the locus, $\Upsilon=\pi/2-\omega$. If the thickness of the crystal is negligible, the spots along the locus will appear as sharp lines. On the other hand, the breadth of a spot is maximum along the locus, $\Upsilon=\pi-\omega$. Between these two extremes, the general expression of spot-breadth, B_{hol}, in Weissenberg photographs may be formulated as follows,

$$B_{hol}=H(\omega,\Upsilon)+\Delta\alpha\,.$$

The first term $H(\omega,\Upsilon)$ is related only to the crystal habit, while the second term, $\Delta\alpha$, is the one due to the vertical divergence of the X-ray beam and constant for a given instrumental set-up. If the cross section of a crystal is a rectangle with edges a and b, the first term is simply expressed by

$$H(\omega, \Upsilon) = C - S$$

where $C = a \cos(\Upsilon - \omega)$ and

$$S = b \sin(\Upsilon - \omega).$$

If a and b correspond respectively to the thickness and the breadth of the crystal, the function $S/b = \sin(\Upsilon - \omega)$ can be shown graphically as shown in Fig. 8. The same chart can be used for evaluating the other term $C/a = \cos(\Upsilon - \omega)$ simply by shifting the origine ($\omega = 0$) of the chart by 90°. Since the cross section of a thin crystal plate can be approximated to a rectangle, the above procedure may be applied to evaluate the distribution of B_{h0l} in the present case. As already discussed by Kaan and Cole[11], the observed intensity I'_{h0l} is, then, related to ideal intensity I_{h0l} as follows,

$$\frac{I_{hl}}{I_{h'l'}} = \frac{B_{hl}}{B_{h'l'}} \cdot \frac{I'_{hl}}{I'_{h'l'}}.$$

Fourier analysis of the structure

As stated above, it would be most reasonable to consider that the structure of the α-form has an orthorhombic symmetry, and it

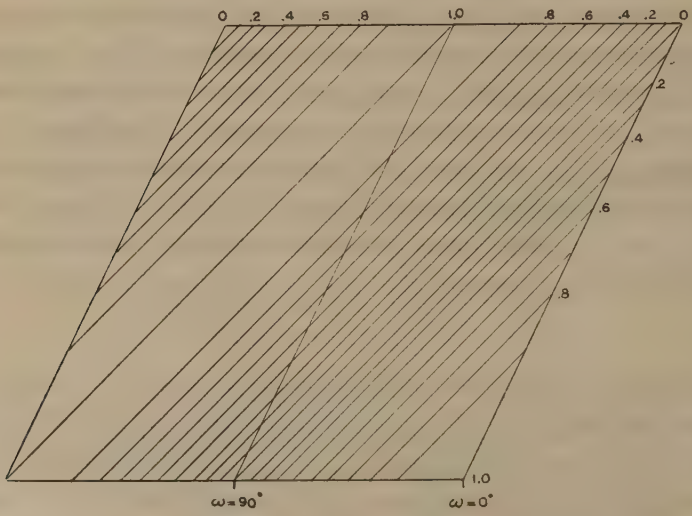

Fig. 8. Numerical numbers indicate the values of $\sin(\Upsilon - \omega)$.

may be expected that the arrangement of the barium atoms has perfect hexagonal symmetry since there are only four atoms in the body centered orthorhombic cell and they must be distributed over a set of special positions. Therefore, deviation from the hexagonal symmetry may be due to the shifts of the rest of the atoms. Although the interpretation of the X-ray data based upon the hexagonal pseudo-cell gives only an avarage structure, it might be possible to deduce from Fourier peaks the atomic positions in an orthorhombic individual. Thus, the Fourier analysis of the avarage structure was carried out and described in the following sections.

c-axis projection

Because of micaceous cleavage after (0001), it was hardly possible to obtain reliable intensity data for I ($hk0$) in Weissenberg photographs. They were recorded in precession films by the use of MoK-radiation and were measured with the aid of a microphotometer.

The results of the measurements showed that, with the atomic coordinates previously reported, the comparison between F_0 and F_c gave the descrepancy facter 10.2%. In view of the presence of barium atoms in the structure, however, the fairly low value of this factor is not really significant and the accuracy of coordinates of the rest of the atoms may be correspondingly low. In fact, when the contribution of barium atoms was subtracted from each of F_0 and F_c, the descrepancy factor for the rest of the structure, namely $|\Sigma|F_0-f_{Ba}|-\Sigma|F_c-f_{Ba}||/\Sigma|F_0-f_{Ba}|$, was found to be 15.1 %.

The F_0-F_c synthesis was, then, calculated and it showed rather high peaks along the a-axis at positions close to (0, $\frac{1}{2}$), thus suggesting shifts of oxygen atoms from that special position. It was found that when the location of the oxygen atom was moved to (0, 0.450), the comparison between F_0 and F_c showed best agreement, the R-factor being reduced to 5.4%. The electron-density projection shows an elongated peak along the a-axis at the positions cor-

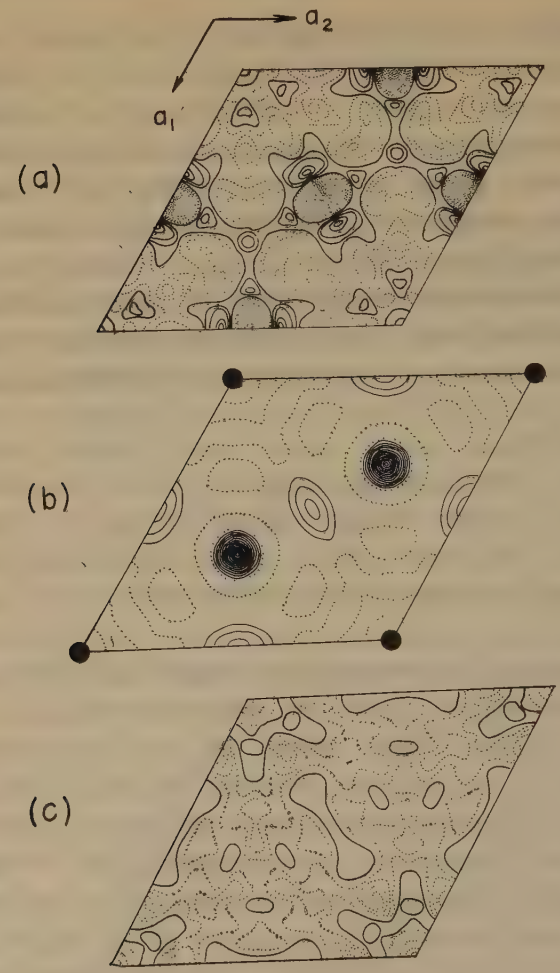

Fig. 9. (a) First difference synthesis projection on (001). Contours are drawn at intervals of 0.6 e.A^{-2}, the dotted contours being zero and negative lines.
(b) Electron-density projection on (001). Contours at intervals of 2e.A^{-2} for oxygen and 4e.A^{-2} for the peaks at 1/3, 2/3 and 2/3, 1/3, zero and negative contours being dotted. Barium atoms are subtracted.
(c) Final difference synthesis projection on (001). Contour intervals are the same as (a).

responding to these oxygen atoms. Regardless the oxygen positions, namely whether they are at $(0, \frac{1}{2})$ or at (0, 0.450), the signs of F ($hk0$)'s were found to be all positive, and, therefore, the shape of peaks in the Fourier map was not affected by the choice of the oxygen position. The first difference synthesis, the Fourier projection and the final difference synthesis are given in Fig. 9a, Fig. 9b and Fig. 9c respectively.

It is now clear that as far as the projection is concerned, the $(Al_2Si_2)O_8$ sheet in the α-form has no longer hexagonal symmetry

Table 1. Comparison of observed and calculated $F(hk0)$'s.
F'_c indicates the structure factors based upon the previous atomic coordinates. $R = |F_0| - |F_c| \div |F_0|$. $R' = |F_0 - F^{Ba}| - |F_c - F^{Ba}| \div |F_0 - F^{Ba}|$. F^{Ba}=Contribution of barium atoms.

$hk0$	F_0	F'_c	F_c	$F_0 - F^{Ba}$	$F'_c - F^{Ba}$	$F_c - F^{Ba}$
100	10.6	8.9	10.5	−41.0	−43.1	−41.5
200	54.8	54.8	52.0	10.3	10.3	7.5
300	76.5	69.5	74.6	39.3	32.3	37.4
400	18.2	31.4	24.8	−12.8	0.4	− 6.2
500	17.3	12.4	19.5	− 8.8	−13.7	− 6.6
600	45.8	53.0	44.5	23.9	31.1	22.6
110	85.5	84.8	86.2	39.3	38.8	40.0
120	10.5	9.9	11.2	−29.0	−29.6	−28.3
130	9.2	9.0	9.4	−24.2	−24.4	−24.0
140	52.9	51.6	58.6	25.1	23.8	30.8
150	9.7	8.9	13.1	−13.8	−14.6	−10.4
220	83.0	90.0	82.3	48.5	55.5	47.8
230	20.6	19.1	20.4	− 7.4	− 8.9	− 7.6
240	20.4	24.1	18.4	− 4.1	− 0.4	− 6.1
250	44.7	37.2	42.3	23.5	26.0	21.1
330	51.0	45.9	49.6	26.0	20.9	24.6
340	10.7	8.8	11.7	−11.0	−12.9	−10.0
R		10.2%	5.4%	R'	15.1%	8.4%

but appears to have a trigonal symmetry as has been found in hexagonal $CaAl_2Si_2O_8$[15]. The comparison between the observed and the calculated structure factors is given in Table 1.

a-axis projection

As stated in the foregoing section it was necessary, in the case of collecting data for this projection, to apply the corrections both for absorption and for spot size. The observed $F^2(h0l)$'s, derived from the intensity data which had been corrected for these effects, were used for computing the Patterson projection. From the observation of the projection, it was revealed that the distribution of peaks in the map is compatible with the atomic arrangement in the a-axis projection of the previous structure which was obtained by trial-

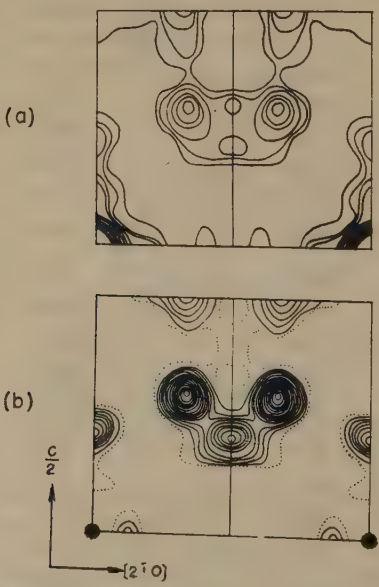

Fig. 10. (a) Patterson projection along a-axis. Contours at arbitrary scale.
(b) Electron-density projection along a-axis. Contours at arbitrary scale. Barium atoms are subtracted.

and-error method. The structure factors were then calculated based upon the previous structure except the O_2 atom for which the newly obtained x-coordinate was employed and only one negative sign was found out of 53 $F(h0l)$ terms. By taking account of the results of F_0-F_c synthesis, the refinement of the atomic coordinates was attempted until the R-factor was reduced to 13%. The coordinates of atoms found at this stage are:

atom	Z	x	y	z
Ba	1	0	0	0
$\frac{1}{2}$Si, $\frac{1}{2}$Al	4	$^1/_3$	$^2/_3$	0.290
O_1	2	$^1/_3$	$^2/_3$	0.500
$\frac{1}{2}O_2$	12	0.450	0	0.210

Fig. 10a and Fig. 10b show respectively the Patterson projection and the corresponding Fourier map based upon $F(h0l)$'s from which the contribution of Ba has been subtracted.

Three dimensional Fourier synthesis

The contribution of barium atoms was subtracted from F_0 (hkl) and the three dimensional Fourier synthesis was computed at inter-

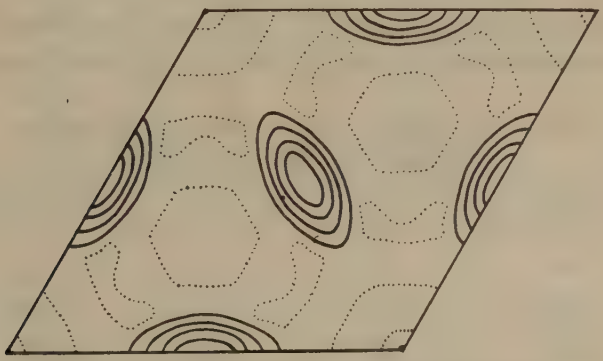

Fig. 11. Fourier section at $z=12/60$. Contours at intervals of 2e.A^{-3}, the dotted contours being zero-electron line.

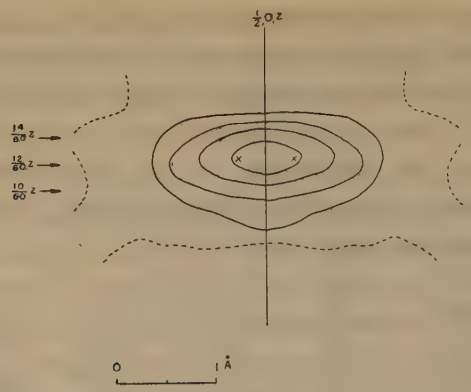

Fig. 12. Part of $(x, 0, z)$-section showing the peak of O_2 atom. Contours at intervals of 2e.A^{-3}, the dotted contours being zero-electron line.

vals of 1/60 of the cell edges. The peak corresponding to O_2 atom is shown in Fig. 11, the section at z=12/60, and in Fig. 12, where part of $(x, 0, z)$-section is given. As shown in these figures, it was not possible to find out the accurate position of O_2 atom owing to lack of resolution. The peak for $Si\frac{1}{2}$, $Al\frac{1}{2}$ and O_1 are fairly well defined (Fig. 13). The line syntheses along $(\frac{1}{3}, \frac{2}{3}, z)$ and $(0, 0.45, z)$ are shown in Fig. 14.

The final atomic coordinates are given in Table 2. In Table 3, the comparison between F_0 and F_c is given. The R-factor found for the final coordinates are R_{h0l}=11.8% and R_{hkl}=12.0 %.

Table 2. Coordinates of atoms found in the avarage structure of α-hexagonal $BaAl_2Si_2O_8$.

atom	x	y	z
Ba	0	0	0
$Al\frac{1}{2}Si\frac{1}{2}$	1/3	2/3	0.288
O_1	1/3	2/3	0.500
O_2	0.450	0	0.209
	0.550	0	0.209

Table 3. Comparison of observed and calculated $F(hkl)$'s.

hkl	F_0	F_c	*hkl*	F_0	F_c	*hkl*	F_0	F_c
000	—	174	401	33.0	40.2	411	15.1	14.9
001	28.5	34.0	402	29.6	32.6	412	10.1	13.4
002	14.4	− 8.2	403	14.1	15.5	413	31.6	35.3
003	37.1	41.8	404	18.0	23.1	414	21.7	31.9
004	91.0	84.5	405	43.5	46.2	415	4.2	0.9
005	17.5	15.4	406	20.4	17.5	416	16.7	17.3
006	25.9	33.1	407	8.4	9.1			
007	35.2	32.4				511	25.8	23.2
008	15.8	16.1	501	29.5	29.8	512	25.0	27.9
009	12.0	18.2	502	24.8	25.7	513	16.6	18.1
0010	37.0	37.3	503	11.0	18.3			
			504	19.7	20.7	221	19.6	21.3
101	68.5	63.6	505	26.8	30.0	222	8.5	2.3
102	75.0	69.0				223	35.0	35.0
103	43.0	38.6	111	25.8	21.4	224	46.2	48.7
104	21.7	20.7	112	35.0	28.6	225	0	1.6
105	41.5	49.0	113	68.0	63.5	226	26.6	25.8
106	24.4	28.3	114	53.2	54.1	227	29.8	29.5
107	16.1	22.7	115	9.8	− 5.4			
108	33.3	29.4	116	29.3	31.3	321	25.1	27.6
109	31.0	26.6	117	46.4	46.1	322	24.9	28.0
			118	16.3	19.7	323	19.5	22.4
201	64.8	58.9	119	7.4	4.6	324	20.1	25.5
202	29.0	26.4				325	38.2	30.1
203	16.1	19.5	211	43.0	43.0	326	14.0	12.5
204	31.4	39.1	212	53.6	49.7			
205	55.0	59.6	213	28.0	28.8	421	25.4	26.0
206	20.8	21.3	214	16.9	18.6	422	24.1	25.2
207	8.6	8.6	215	24.0	38.8	423	14.9	15.2
208	18.4	27.8	216	20.7	24.3	424	16.5	16.3
209	31.9	34.0	217	15.7	18.7			
			218	20.5	24.5	331	13.4	13.6
301	18.7	20.1				332	9.6	15.4
302	14.5	17.0	311	35.9	35.0	333	20.5	17.9
303	41.4	49.0	312	37.8	41.7	334	30.4	31.4
304	45.2	46.8	313	21.8	23.8			
305	0	− 1.2	314	12.2	16.2			
306	29.4	32.4	315	25.9	33.1			
307	34.1	38.4	316	19.8	21.9			
308	15.3	19.7	317	16.4	17.4			

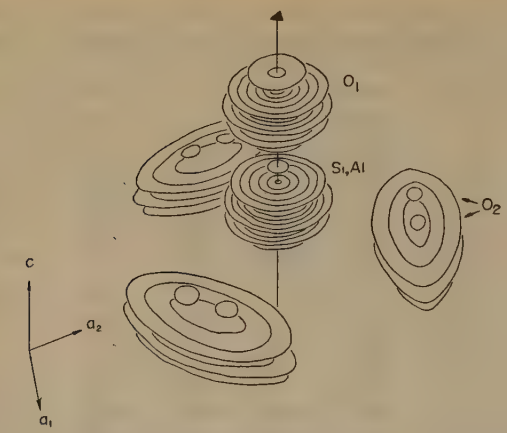

Fig. 13. Composite electron-density showing one Si(Al) O_4 tetrahedron. Contours at intervals of $2e.A^{-3}$ for oxygen atoms and at $4e.A^{-3}$ for (Si, Al) atom, starting at $2e.A^{-3}$.

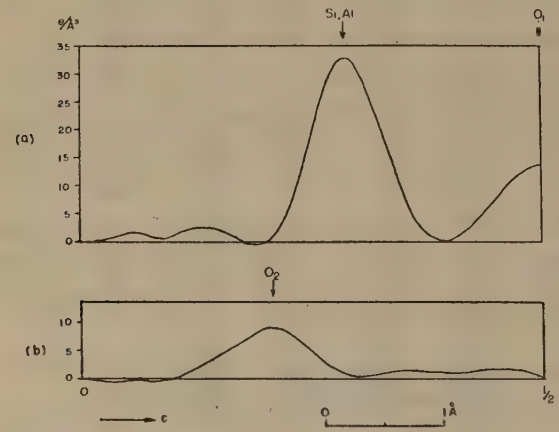

Fig. 14. The line syntheses along (1/3, 2/3, z) (a) and (0, 0.45, z) (b).

Discussion

The final atomic coordinates show that the structure is composed of $(Al_2Si_2)O_8$ sheets of trigonal symmetry. If two such layers in a cell are symmetrically so related that one layer is brought

into coinsidence with the other by a rotation of 180° followed by a translation of $c/2$, the resulting structure will have the space group D^3_{6h}*, the lattice constants being a_0 and c_0. The $(Al_2Si_2)O_8$ sheets in the α-form, however, would be slightly deformed from the perfect trigonal symmetry in such a way that the stacking of these sheets give rise to a motive of body centered orthorhombic lattice, which is strongly suggested by the broad peak corresponding to O_2 as found in the three-dimensional synthesis. In Fig. 15, the projection of the avarage structure is shown as the alternating stacking of the $(Al_2Si_2)O_8$ sheets with trigonal symmetry.

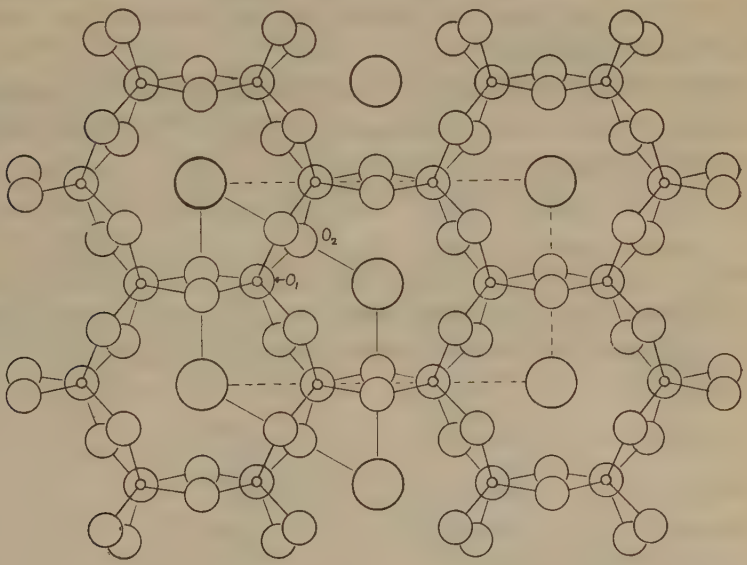

Fig. 15. Arrangement of atoms in the c-axis projection. Hexagonal and orthorhombic cells are outlined by solid and broken lines respectively.

Although the structure of hexagonal $CaAl_2Si_2O_8$ and that of hexagonal $BaAl_2Si_2O_8$ are composed of similar sheets, there are

* It has been found that hexagonal $CaAl_2Si_2O_8$ has exactly the same type of this structure[15].

stacking mistakes of the sheets in the calcium compound, while trilling of the orthorhombic structures occurs in the barium analogue. This difference may probably be due to a slight difference in the configurations of the constituent sheets. Namely, the symmetry of the sheet in the α-form is orthorhombic, requiring the unique succession of the sheets, while the sheets in hexagonal $CaAl_2Si_2O_8$ are trigonal, permitting themselves to stack in various ways. These situations are somewhat similar to the structural differences between muscovite and biotites. Hendricks and Jefferson has suggested that the configurations of mica sheets in muscovite are different from those in biotites and this leads to the unique structure of muscovite[7].

In the structure, Ba atoms are surrounded by six oxygen atoms octahedrally with the equal distance of 2.89 Å. The value agrees well with the mean value of the Ba-O distances found for paracelsian[13]. As shown in Table 4, the Ba-O distances in some of the

Table 4. Ba-O distances in some of the barium compounds.

substance	chemical formula	Ba-O distance	No. of neighbouring oxygen atoms
α-hexagonal $BaAl_2Si_2O_8$	$BaAl_2Si_2O_8$	2.89 3.34	6 6
paracelsian[13]	$BaAl_2Si_2O_8$	2.89* >3.3	5 2
sanbornite[3]	$BaSi_2O_5$	2.87* 3.14	7 2
gillespite[12]	$BaFeSi_4O_{10}$	2.86*	8
barium titanate[5] (tetragonal)	$BaTiO_3$	2.834*	12
baryte[10]	$BaSO_4$	2.83*	12
barium oxide[6]	BaO	2.75	6
hollandite[2]	$(Mn,Fe)BaMn_6O_{14}$	2.74 3.31	8 4
benitoite[18]	$BaTiSi_3O_9$	2.74	6
dibarium cupric[14] formate tetrahydrate	$CuBa_2(COOH)_8 \cdot 4H_2O$	2.74	6

Mean values are indicated by asterisks.

barium compounds are around 2.74 Å which corresponds to the sum of Goldschmidt's ionic radii and some of them shows much larger Ba-O distances. It is interesting to note that, in the compounds composed of silicate sheet structures, the Ba-O distances have invariably larger values.

The distances between the other atoms are:

$Si_{\frac{1}{2}}Al_{\frac{1}{2}}-O_1$	1.65 Å
$Si_{\frac{1}{2}}Al_{\frac{1}{2}}-O_2$	1.67
O_1-O_2	2.75
O_2-O_2	2.69

Since these values are based on the three-dimensional Fourier analysis of the *avarage structure*, the estimation of the accuracy in bond length was not made.

Structure of β-form and α-β inversion

Powder patterns

Powder diffraction patterns of the β-form was taken at about 450°C. using a furnace which was mounted on the Norelco Diffractometer in place of the standard sample holder. No significant dif-

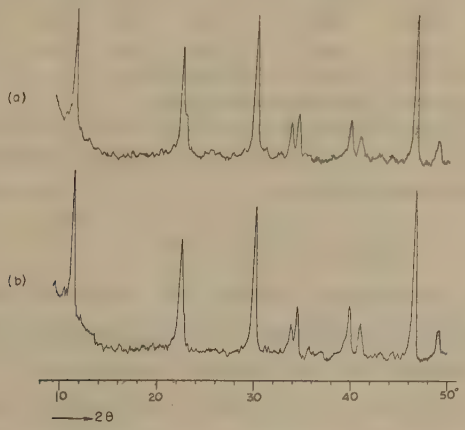

Fig. 16. Powder diffraction patterns, (a) β-form, (b) α-form.

ferences are observed between the powder patterns of the α- and the β-form except peak shifts owing to lattice expansion, indicating the fundamental frame works of the both structures are same, and it is expected that the change of the structure is confined to slight shifts of light atoms. The powder peaks of the β-form can be indexed by a hexagonal cell with constants, a=5.313 and c=7.805 Å, and they are listed in Table 5 where the powder data of the α-form are compared.

Table 5. X-ray powder diffraction data for hexagonal $BaAl_2Si_2O_8$. Observed and calculated Q-values are compared.

α-form				β-form				
d_{obs}	I*	Q_{obs}	Q_{calc}	d_{obs}	I*	Q_{obs}	Q_{calc}	hkl**
7.79	100	.0164	.0165	7.79	112	.0165	.0164	001
3.949	43	0641	0641	3.963	47	0637	0637	101
3.899	18	0658	0659	3.901	20	0657	0657	002
2.968	49	1135	1135	2.977	59	1128	1129	102
2.647	13	1427	1427	2.659	15	1414	1417	110
2.597	20	1483	1483	2.602	22	1477	1477	003
2.292	4	1903	1903	2.300	5	1890	1890	200
2.259	18	1960	1959	2.266	15	1947	1950	103
2.195	11	2075	2068	2.206	11	2055	2054	201
1.947	65	2638	2637	1.951	60	2627	2627	004
1.853	7	2912	2910	1.860	6	2890	2894	113

* Specimens show preferred orientation.

** Powder peaks of the α-form can be indexed by the hexagonal pseudo-cell because the weak extra reflexions are not observed in the powder patterns.

High temperature oscillation photographs

Oscillation photographs around the c-axis of the β-form were taken at about 500°C. utilizing a high temperature powder camera which was modified for oscillation photography. An interesting result on the structure of the β-form was found. Namely, the weak spots on the positions corresponding to odd layers disappeared in

the high temperature photographs. This means that the body-centered orthorhombic structure in the α-form had changed into a hexagonal structure, thus indicating that the $(Al_2Si_2)O_8$ sheets have hexagonal symmetry in the β-form. It would, therefore, be concluded that the β-form has hexagonal cell with constants (at about 450°C.), $a=5.313\pm0.05$ Å and $c=7.805\pm0.05$ Å, and with space group D^1_{6h}.

The change of the structure at the transition temperature may be depicted in a way as shown in Fig. 17.

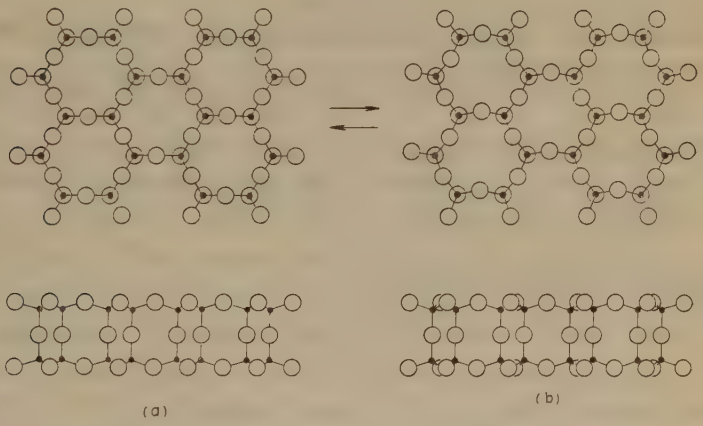

Fig. 17. Configurations of $(Al_2Si_2)O_8$ sheet.
(a) β-form (above 300°C.)
(b) α-form (below 300°C.)
In each case the upper diagram shows a view along the normal to the sheet, while the lower diagram gives a section along the a-axis.

I am grateful to Professor T. Ito and Dr. R. Sadanaga for helpful discussions.

References

1) Buerger, M.J.: Z. Krist., **99**, 189 (1938).
2) Byström, A. and Ann Marie Byström: Acta Cryst., **3**, (1950).
3) Douglass, R.M.: Am. Mineral., **43**, 518 (1958).
4) Davis, G.L. and O.F. Tuttle: Am. J. Sci., Bowen Volume, 107 (1952).
5) Evans Jr, H.T.: Acta Cryst., **4**, 373 (1951).
6) Gerlach, W.: Zeit. f. Phys., **9**, 184 (1922).
7) Hendricks, S.B. and M.E. Jefferson: Am. Mineral., **24**, 729 (1939).
8) Ito, T.: *X-Ray Studies on Polymorphism*, Tokyo, Maruzen (1950)
9) Joel, N., R. Vera and I. Garaycochea: Acta Cryst., **6**, 465 (1953).
10) James, R.W. and W.A. Wood: Proc. Roy. Soc., A **109**, 198 (1925).
11) Kaan, G. and W.F. Cole: Acta Cryst., **2**, 38 (1949).
12) Pabst, A.: Am. Mineral., **28**, 372 (1943).
13) Smith, J.V.: Acta Cryst., **6**, 613 (1953).
14) Sundara Rao, R.V.G., K. Sundaramma and G. Sivasankara Rao: Z. Krist., **110**, 231 (1958).
15) Takéuchi, Y. and Gabrielle Donnay: C.R. Acad. Sci. Paris, **248**, 265 (1959).
16) Takéuchi, Y.: Mineralogical Jour., **2**, 162 (1957).
17) Yoshiki, B. and K. Matusmoto: Am. Ceramic Soc. Jour., **34**, 283 (1951).
18) Zachariasen, W.H.: Z. Krist., **74**, 139 (1930).

Manuscript received Oct. 20, 1958.

Mineralogical Journal, Vol. 2, No. 5, 333-335, Dec., 1958

SHORT COMMUNICATIONS

LITHIAN BIOTITE FROM THE TAKATORI MINE, IBARAGI PREFECTURE*

Toshio Kato

Mineralogical Institute, University of Tokyo

A lithia mica was collected during my visit to the Takatori** mine, Ibaragi Prefecture, in 1954, and subsequent study have revealed that this mica belongs to lithian biotite.

Occurrence and general properties. The Takatori mine is situated about thirty kilometers northwest of Mito city. The region is composed of Palaeozoic system which consists mainly of sandstone, slate and chert. The mine is working wolframite which occurs in high temperature type quartz veins filling the fissures in these sedimentary rocks. The lithia mica was found as masses filling a cavity in the wall rock of reddish brown coloured sandstone at Akabokke-hi*** in the Takatori mine. The principal minerals associated are yellowish green coloured topaz, quartz, fluorite, cassiterite and sulfide minerals such as pyrite and arsenopyrite.

The lithian biotite is silver grey to silver brown in colour. Their cleavage flakes have a silver white colour and are flexible. Pleochroism distinct: X yellow, Y and Z dark brown. The refractive indices: $\alpha=1.568$ $\beta\fallingdotseq\gamma=1.597$. Apparent optic angle of crystal aggregate of the mica is zero to very small: optically negative. The specific gravity was determined as 3.10 at 18°C. by means of

* Read at the Annual Meeting of the Mineralogical Society of Japan held in Tokyo in June, 1955.

** 高取鉱山. *** 赤木毛鑓.

picnometer.

Chemical composition. The sample for chemical analysis was separated by means of hand picking and then of isodynamic separator to remove trace amount of sulfide. Spectroscopic analysis revealed that the sample did not contain noticeable amount of element other than those chemically analysed. Rubidium was not detected by the X-ray fluorometric analysis, too. They were analysed by the ordinary method. Its chemical composition is as follows:

SiO_2 37.48, TiO_2 0.06, Al_2O_3 20.58, Fe_2O_3 2.43, FeO 19.54, MnO 2.01, CaO 0.38, MgO 1.60, K_2O 9.94, Na_2O 0.21, Li_2O 1.32, H_2O (+) 2.44, H_2O(−) 0.89, F 1.92, −O 0.82, total 99.98%.

(Analyst T. Kato, 1955)

This chemical composition can give the following structural formula based on the negative charge as 22,

$(Ca_{0\cdot03}Na_{0\cdot03}K_{0\cdot96})$ $(Li_{0\cdot40}Mn_{0\cdot13}Mg_{0\cdot18}Fe^{\cdot\cdot}{}_{1\cdot23}Fe^{\cdot\cdot\cdot}{}_{0\cdot14}Al_{3\cdot60})$ $(Al_{1\cdot24}Si_{2\cdot76})$ $O_{10}[(OH)_{1\cdot29}F_{0\cdot48}]$.

Chemically the lithia mica is characterized by the considerable high percentage of MnO and the defficiency of divalent cations.

It has been suggested by Heinrich et al.[2] that the lithian iron mica with less than one Li (calculating the formula on the basis of O, OH+F=24) be classified as lithian biotite. Although the characteristics of the lithia mica from Takatori agrees those of the so-called protolithionite[4], the writer is inclined to classify the mica from Takatori as lithian biotite according to Heinrich's proposal.

X-ray powder diffraction data. X-ray powder diffraction data for the specimen analysed chemically was obtained by Phillips Geiger counter X-ray diffractomter (Table 1). The data agrees closely with those of iron biotite[1][3].

Acknowledgements. The writer wishes to express his sincere thanks to Prof. T. Ito for his guidance and also to Prof. N. Katayama for his critically reading the manuscript. The writer also greatly

Table 1. X-ray powder diffraction data for lithian biotite from the Takatori mine, Ibaragi Prefecture. (Cu$K\alpha$ radiation)

hkl	*d*	*I*	*hkl*	*d*	*I*
001	10.2 Å	100	006	1.670 Å	6
002	5.08	4		1.533	4
	3.71	3		1.463	3
003	3.34	70		1.455	3
200	2.622	6		1.427	4
004	2.522	10		1.361	3
	2.191	5		1.307	4
005	2.002	10		1.248	5

indebted to Dr. H. Minato, Dr. K. Sakurai, Mr. I. Fujii and Mr. A. Sasaki for their kind help and suggestions during the study.

References

1) Grim, R.E.: Clay Mineralogy, New York (1953).
2) Heinrich et al.: Rept. University of Michigan Engineering Research Institute (1953).
3) Nagelschmidt, G.: Z. Krst., 97, 519 (1937).
4) Ukai, Y. et al.: Miner. Jour., 2, 27 (1957).

Manuscript received Nov. 15, 1958.

ABSTRACT OF THE KOBUTSUGAKU ZASSHI,

JOURNAL OF THE MINERALOGICAL SOCIETY
OF JAPAN, VOL. 3, NO. 6,
September, 1958

Jubilee Number Dedicated to Prof. Z. Harada in Celebration
of His Sixtieth Birthday

Bementite and Pyroxmangite from the Ichinomata mine, Kumamoto Prefecture (pp. 457-467)

Toyofumi Yoshimura, Haruo Shirozu and
Fumitoshi Hirowatari

The material was collected from the manganese ore deposit of the Ichinomata mine, situated 18 km. south of Yatsushiro City, Kumamoto Prefecture. Associated minerals are rhodochrosite, tephroite and hornstone-quartz.

Bementite forms semitransparent masses with various shades of brown. Under the microscope, it is observed as practically monomineralic aggregate of very minute flakes of bementite. H=5½, d=3.03, $\alpha'=1.631$, $\gamma'=1.633$, $\gamma'-\alpha'=0.002$.

Pyroxmangite is a minor constituent of the siliceous manganese ore of this mine. It occurs as porcelain-like masses with pinkish grey colour. Under the microscope it is very finely granular. In places it appears as minute fibrous crystals, arranged radially and spherulitic. H=6, d=3.26, $\alpha=1.717$, $\gamma=1.732$.

X-ray powder photographs, chemical compositions and d. t. a. curves were examined on the two minerals and problems concerning their relations to ganophyllite and rhodonite respectively were discussed to a certain extent.

Nickeliferous Clay Mineral from Niû Mine, Oita Prefecture (pp. 468-477)

Kameki Kinoshita, Nobuya Tanaka and Tsuneo Honda

The authors have treated pale-blue soft clay mineral collected from Niû Mine in Ôita Prefecture as an item of their studies on nickeliferous silicate minerals. This mineral was temporarily called "garnierite", but it has been discovered through a couple of experiments that garnierite has properties different from it and that it is equivalent to nickel montmorillonite, in which the nickel replaces a part of magnesium.

The accompanying minerals are kaolinite (not quite certain), dolomite and opal. Both dolomite and opal contain a small quantity of nickel, but the greater part of the nickel seem to be contained in nickeliferous montmorillonite according to analytical results.

Mode of Occurrence and Chemical Composition of Mg-vermiculite from Odaka and Uzuminé, Fukushima Prefecture (pp. 478-485)

Keiichi Omori

Mg-vermiculite occurs associated with anthophyllite or asbestos and talc in narrow belts at the margin of serpentine in contact with pegmatites at several places in Odaka and Uzuminé, Fukushima Prefecture. Based on the chemical analyses by H. Konno the chemical formulae of the specimens from Odaka and Uzuminé are calculated as $Mg_{0.37}$ $(Mg_{2.17}$ $Ca_{0.01}$ $Mn_{0.01}$ $Fe_{0.51})$ $(Si_{2.75}$ $Al_{1.22}$ $Ti_{0.02}$ $Fe_{0.01})$ $O_{10}(OH)_2 \cdot 3.90(H_2O)$ and $Mg_{0.36}$ $(Mg_{2.60}$ $Fe_{0.10})$ $(Si_{2.85}$ $Al_{1.08}$ $Ti_{0.03}$ $Fe_{0.04})$ $O_{10}(OH)_2 \cdot 4.59(H_2O)$ respectively.

Maghemite from Takanokura Mine, Fukushima Prefecture (pp. 486-491)

Tsunehiko Takeuchi and Matsuo Nambu

Supergene maghemite associated with hematite and goethite, occurs in the weathered surface of the contact-metasomatic magnetite deposits

of Takanokura Mine, Fukushima Prefecture, Japan.

The mineral is identified by chemical analysis, X-ray powder analysis and differential thermal analysis. Oxidation process of the Takanokura iron oxide minerals are assumed as follows:

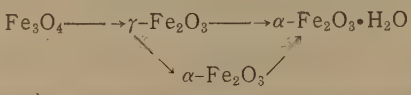

Studies on the Impurities in Metallic Selenium with Special Reference to the Properties as a Rectifier

(pp. 492-513)

Tadao Saito

In order to clarify the rectifying action of metallic selenium, the author studied the minor impurities contained in it and the temperature effect on its crystal texture.

Minor impurities when added to selenium increase the electro-conductivity of selenium, and embody various nature as a semiconductor. And heat treatment gives rise to generation of kernel and growth of hexagonal crystal and of blocking oxide layer. The temperature and duration of heat treatment are controling factors of the rectifying action of selenium, and remarkably effect the forward current and reverse voltage.

The rectifying phenomena of selenium may be due to the behaviour of positive holes against the potential wall which is derived from high resistance of the blocking oxide layer produced on the selenium surface.

Crystallization of Volcanic Glass by Alkali Solutions

(pp. 514-522)

Toshio Sudo and Masachika Matsuoka

By digesting glassy tuff with alkaline solutions on the waterbath, the writer obtained sodalite and a zeolitic material. Studying in detail the products obtained by the reactions of glassy tuff with NaCl and NaOH solutions in various concentrations, the writers confirmed the conditions favourable for crystallization of these materials. The longer the tuff was warmed in more concentrated solutions, the more sodalite was produced

Crytallization of the zeolitic material is favourable in the case of lower concentrations of these solutions. NaOH solution seems to behave as a catalyst for the crystallization courses.

On the Rubidium and Cesium in Carnallite (pp. 523-532)

Shunji Matsuda

The enrichment of rubidium and cesium in carnallite has been pointed out by many workers.

The behaviour of trace amount of rubidium and cesium during the crystallisation of halite, sylvite, bischoffite and carnalite, was studied by isothermal evaporation of each of the saturated solution by use of ^{137}Cs and ^{86}Rb as tracer.

Logarithmic distribution coefficients of rubidium and cesium between the crystal and the solution have been determined as follows: logarithmic distribution coefficient of rubidium in halite is 0.14; in sylvite, 0.4, in bischoffite, 0.3; and in carnallite, 2.4; and that of cesium in halite, 0.02; in sylvite, 0.03; in bischoffite, 0.3 and in carnallite, 1.3. Those results suggest that rubidium and cesium will be selectively concentrated in carnalite among the oceanic salts.

Two specimens of natural carnalite from the salt deposit in Stassfurt were studied by chemical analysis and X-ray powder method, and it was revealed that one of the samples was the mixture of carnallite, halite and kainite, and the other was a pure carnallite; and that the former contained 1 ppm. of cesium while the latter 2 ppm.. The Rb/Cs ratio of the former was 90 and that of the latter was 85.

Studies of Limonite Ore from the Shinmei Mine, Hokkaido (pp. 533-538)

Kazuo Adati and Yu Hariya

Chemical, X-ray and thermal analyses as well as microscopic observation data are given for some specimens of limonite ore from the Shinmei mine, Hokkaido, Japan. The Nakanosawa ore deposit of this mine is of impregnate or metasomatic type formed in Neogene Tertiary sediment. Principal lines in X-ray powder patterns of the limonite ore are in accor-

dance with those of goethite. Crystallinity of these goethite differs in parts of the ore bodies.

Chromian Enstatite from Hirosé Mine, Tari District, Tottori Prefecture (pp. 539-542)

Jun-ichi Kitahara

Enstatite occurs with andradite filling a fissure of pyroxenite and chromite ore body at the Ôgiri level of Hirosé Mine, Tari district, Tottori Prefecture.

The crystals are (010) tabular with (100), (010) and (101) faces. The specific gravity is 3.234 and the hardness is $5\frac{1}{2}$. The crystals are pale green and sub-transparent. In thin section, the mineral is colourless and the optical plane is (100). Optical properties: $\alpha=1.667$ and $\gamma=1.672$; $(+)2V=61.5°$. The chemical composition is given as follows: SiO_2 54.01, TiO_2 0.03, Al_2O_3 3.95, Fe_2O_3 2.07, Cr_2O_3 0.57, FeO 1.57, MnO 0.00, CaO 0.99, MgO 35.65, NiO 0.09, K_2O 0.00, Na_2O 0.08, $H_2O(\pm)$0.59, total 99.60 (wt%).

Crystal Growth of Hematite from Ayumikotan, Japan (pp. 543-556)

Ichiro Sunagawa

On the basal plane of one crystal of hematite from an andesitic lava at Ayumikotan, Japan, three types of growth pyramids are described.

First type, which is called the "tetrahedral" growth pyramid, consists of many closely spaced, thin, concentric, equi-lateral triangular growth layers. On some of these growth pyramids spiral growth and interlacing can be observed. On some growth pyramids of this type the layers on one side of the triangular are produced into a peak suggesting the presence of an imperfect screw dislocation. Multiple beam interferometry and fringes of equal chromatic order show that the thinnest growth layers are 2.3Å thick (1/6 of the thickness of the unit cell).

Second type is called the "triangular" growth layer. They are equilateral triangular growth layers on which no spirals have been observed. It is suggested that the layer growth took place by two-dimensional neucleation. The origin of the structure within the triangles and the

linear arrangement of growth centres is described. At some distance from the growth triangles, a serrated structure, like saw-teeth, is developed.

In the third type of growth pyramids the thickness of the layers in different cases varies from 1 to 4 unit cells including thickness of $\frac{2n+1}{2}$ unit cells. These growth pyramids seem to be formed by screw dislocation, as there is a pit at the centre of each growth pyramid. The type of interlacing shown by these growth pyramids suggests that polytypism may be present.

From these observations it is deduced that this crystal has grown under the condition of comparatively high supersaturation.

Stalactite from the Ezobanryu Limestone Cave Toma-mura, Hokkaido (pp. 557–564)

Masaru Goto

So-called "tube stalactite" found in the Ezobanryu cave form a monocrystalline or nearly monocrystalline slender tube, elongated along the c-axis of calcite crystal. Almost all of the tube stalactite are about 4.5 mm. in diameter. As to the lateral growth of this tube, three kinds of mode are observed.

1) When the velocity of the lateral growth is extremely slow, the tube grows into an adult "monocrystalline stalactite", keeping its initial crystallographic orientation.

2) When the velocity is rapid, new nuclei develop on the wall of tube and begin to grow radially. The c-axis of each new crystal is nearly perpendicular to the axis of the tube. The horizontal section of such stalactite looks very much like sunflower.

3) It is observed that in an intermediate case the velocity allows the growth of the tube itself together with the development of new nuclei on it until it is enveloped in newly developing crystals. Such stalactite is named "star stalactite".

Some Manganese Dioxide Minerals in Hokkaido and Their Geological Occurrence (Studies on Manganese Oxide Minerals, Rept. 2)

(pp. 565-591)

Yu Hariya

The manganese mineralization in Hokkaido took place in three different ages, the older one being of Palaeozoic or Mesozoic ages, and the younger two of Miocene and Quaternary. Workable manganese deposits are mostly of Miocene age and distributed only in south-western Hokkaido.

In Hokkaido, manganese dioxide or hydroxide minerals occur usually in a finely grained massive state, and comprise several modifications. Some members are well crystallized but others are of very poor crystallinity. The d.t.a. curves of pyrolusite, manganite, cryptomelane and their mixtures were examined and they gave very useful information on the mineral composition of manganese ores. The writer found pyrolusite, manganite, cryptomelane, ramsdellite, birnessite and ranceite in Hokkaido. Ramsdellite was found for the first time in Japan from the Tanno mine, Kitami District, in a fissure in Palaeozoic red chert beds. Birnessite and ranceite are found in manganese wads from the Komagadaké mine.

In the Pirika type bedded manganese deposit in south-western Hokkaido, a type of zonal arrangement is observed, manganite predominating in the lower bed while pyrolusite in the upper.

Preliminary Note on the Clay Iron-Stone in the Horokabetsu Formation in the Ishikari Coal Field

(pp. 592-596)

Shigeo Ikegami

Clay iron-stones are found in the dark grey thin-bedded shale of the Palaeogene Horokabetsu Formation in the Ishikari Coal Field, Hokkaido. In the vicinity of outcrop the surface of them is altered to limonite. They are in the form of lenses, nodules or beds with a thickness of 50 or 60 cm. in maximum, and so distributed as to make a band parallel to the stratification. The formation contains more than ten such bands.

Essential mineral is siderite, and accessories are quartz, calcite, plagioclase, chlorite and pyrite. Angular quartz and calcite veinlets are very common.

It seems that iron in those iron-stones is of syngenetic origin and siderite has been formed in the course of diagenetic differentiation under moderately high redox potential.

On Iron Sulphides in Calcareous Nodule (pp. 597-602)

Masao Isibasi

At one locality near Sapporo a grey, soft and muddy sedimentary facies enclosing calcareous nodules with iron sulphide minerals are found in the "Misumai-shale" of the Yakumo-series of upper Miocene. The nodules are composed of crystals of iron sulphide and grey, coarsely grained impure calcites. Minerals of iron suphide are pyrite, marcacite and pyrrhotite, which are determined by the mineragraphic studies. These iron sulphides occur forming thin crusts, disseminated grains and star-cloud like patches, or cube like metallic nuclei with curved surface in the nodules.

The properties of iron sulphides have a definite correlation with the mode of occurrence, but not with the shapes, nor sizes of nodules. The outer side of the crust and the nucleus consits of idiomophic pyrites, but the inner side is composed of aggregates of fine pyrite and marcacite or marcacite only. Pyrrhotites are found as hexagonal plate or prism, and distributed in the inner part of nodules, or scattered in the nucleus of calcite or along the peripheral margins of it which have been recrystallized from dark impure calcite.

It seems that during diagenetic processes iron sulphides crystallized out from melnikovitic substances which had been precipitated into muddy sediments in a closed stagnant basin with clouds of calcareous micro-organisums. The most important influence affecting composition of iron sulphides may be the available amounts of sulphur supplied mainly from out side of nodules as hydrogen sulphide, which is the decomposed product of organic matter and contained in bottom water and sediment.

On the Artificial Cristobalite (pp. 603-608)

Toshiro Kagami

It is very effective for making artificial cristobalite to dip calcined quartz into an alkali carbonate solution. It makes the reagent distribute homogeneously through calcined quartz to speed up transition to cristobalite. When treated with 2% solution of $NaHCO_3$ the transition becomes several tens times as speedy as in the case without the treatment.

Dielectric Phenomena of Low Quartz (pp. 609-625)

Ryôiti Kiriyama and Shichio Kawai

Temperature and frequency dependences of the dielectric constant and loss of a transparent single crystal of Brazilian quartz were measured for directions both parallel and perpendicular to its c-axis in the temparature range from -70° up to 600°C., and in the frequency range between 0.3 kc. and 3 Mc., with C. R. bridge and Q-meter. Direct current electric conductivity was also measured at temperatures up to 500°C.. The enthalpy of activation for the dielectric relaxation was 21.3 kcal/mole and the activation energy for the d. c. conduction was 17.84 kcal/mole.

Infrared absorption spectra of the Brazilian quartz and a smoky quartz showed marked dichroism in the neighbourhood of O-H stretching vibration, 2.7~3μ, in every case, but absorption feature was distinctly different from each other.

To compare these data with those of other silicate minerals, electric measurements were carried out for smoky quartz, vein-quartz, beryl and cordierite.

The most probable explanations for the molecular mechamism of such electric phenomena of quartz are deduced as follows:

1) Water molecules or OH ions and Na ions are trapped in some lattice defects being surrounded with certain anisotropic crystalline fields.

2) When the temperature is raised and an external electric field is applied, the water molecule will be orientated loosening the binding interactions due to O-H···O type hydrogen bonds and an ion-dipole interaction between $Na\text{-}OH_2$. This energy of activation is about 21 kcal/mole.

3) Just then the Na ion may be diffusible to the direction of external field breaking away from the restriction. Therefore, the activation energy of diffusion is almost identical with that of the dielectric relaxation.

4) Direct current conduction does not necessarily imply long-range diffusion of ions, but may appear as the result of successive, relative displacement of ion in the lattice. This activation energy must be smaller than that of diffusion. It may correspond to the activation energy of d.c. conduction of about 18 kcal..

Deweylite from Horokanai-mura, Hokkaido

(pp. 626-633)

Hideo Minato and Hisashi Muraoka

Deweylite, a hydrous magnesium silicate, occurs in serpentine region in Horokanai-mura, Uryu-gun, Hokkaido. It is yellowish or brownish in colour and forms masses with small druses. Hardness: 2~3. Brittle and with small cracks. Fracture: conchoidal. Translucent. Luster: vitreous or greasy. Under the microscope, it shows spherulitic texture or granular aggregate and practically isotropic or weakly birefringent. Indices of refraction are lower than 1.54. Decomposed by hydrochloric acid. Chemical analysis of the purified material follows: SiO_2 41.62, TiO_2 none, Al_2O_3 0.06, Fe_2O_3 0.03, FeO 1.35, MnO trace, MgO 33.89, CaO 0.06, H_2O (+) 17.60, H_2O (−) 6.13, total 100.74% (analysed by H. Minato in 1958). It contains Mn, Ti and Ni as trace elements while V, As, Sb, P, Cu, Zn, Cr and Co are not dectected by spectroscopic analysis. Thermogravimetric analysis was carried out as well. X-ray powder pattern of the specimen agrees with that of the deweylites from Yagiyama, Fukuoka Prefecture and from Delaware, New York.

Ferri-Phlogopite from Teshirogi District, Fukushima Prefecture

(pp. 634-639)

Miyoji Sambonsugi

The pegmatite in Teshirogi district has been studied by the writer since 1950. Recently the writer found a characteristic brown coloured mica in some pegmatite. From its chemical composition $[(K, Fe, Mg)_3(Al, Si)_4$

O_{10} (OH, F)] and optical properties [(−)2V=12°, α=1.558, γ=1.601, pleochroic with X=yellow to colourless, Y=yellowish brown, Z=golden brown, X<Y<Z.] it belongs to phlogopite clan. Therefore the writer proposed the name ferri-phlogopite for the mineral.

On Maghemite from the Kumano Mine, Yamaguchi Prefecture and its Oxidation by the Heating (Report I) (pp. 640-659)

Goro Shibuya

The Kumano mine is situated in Susa Town of Yamaguchi Prefecture, and is exploiting a metasomatic deposit in the contact zone of quartz-diorite and limestone. The primary ore consists mainly of magnetite, but having suffered from secondary oxidation or hydrous oxidation remarkably, almost all the ore is changed into maghemite and hematite with lepidocrocite and goethite. Several specimens of maghemite which show various degree of deficiency, are heated at 300°, 450°, 600°, 800° and 1000°C. in air respectively. Heated products were studied by X-ray and chemical method. Referring to the results of differential thermal analysis, the oxidation process of maghemite which includes magnetite is suggested as follows: (1) generation of vacancy in octahedral coordination position, (2) movement of Fe^{3+} ions in tetrahedral coordination position to octahedral one, (3) change of lattice symmetry from cubic to rhombohedral. These three processes are concerned with each other and at the end of oxidation, hematite only is recognizable. The higher the degree of deficiency, the lower the temperature of the last exothermic peak in d.t.a. curves.

On Some Special Minerals in the Kamuikotan Crystalline Schists (pp. 660-673)

Jun Suzuki

The Kamuikotan metamorphic complex develops as irregular long zone between the Mesozoic and Cenozoic formations along the western side of the Hidaka mountain ridge in Central Hokkaido. It runs about 200 km. in a direction of nearly north to south, from areas of boundary of Teshio and Kitami Province.

In general the normal Kamuikotan complex is made up of the products due to slight regional metamorphism, in which the chief petrological members are black siliceous schists and next comes an abundance of green schists. Small amounts of quartzite, phyllite, mylonite and crystalline limestone are intercalated in the complex. From the geological and petrographical points of view, it may reasonably be assumed that the Kamuikotan complex can be readily correlated with the Franciscan formation in California.

Comparatively large lenses or belts of the ultra-basic rocks run parallel to the trend of the Kamuikotan complex. It is noticeable that various interesting crystalline schists locally develop between the normal schistose rocks of the Kamuikotan complex and the ultra-basic intrusives, which have attracted special attention because of the presence of some special minerals, especially soda-bearing silicates. These special rocks may be a product brought about by contact metamorphic action due to ultra-basic intrusion and occurrence of the special minerals in them originated from pyrometasomatism, primarily owing to the action of some especially soda-rich hydrothermal solution derived from the ultra-basic intrusions.

This paper gives an outline of these several special minerals in the pyro-metasomatized rocks, with special reference to the following members; (A) glaucophane and crossite, (B) riebeckite and crocidolite, (C) aegirine-augite, (D) stilpnomelane, (E) piedmontite, (F) garnet, (G) lawsonite and (H) pumpellyite.

Apparent Polytypism and Apparent Cleavage in Micas

(pp. 674-692)

Yukio Takano and Kotoyo Takano

The authors determined the crystal structure of xanthophyllite from the Chichibu mine, which is iso-structural with 1M type muscovite. The xanthophyllite is found only as twinned crystals. The hexagonal plates, which consist of three or six twinned pieces are stacked together vertically as a parallel growth or a polysynthetic twin, holding c*-axis in common. Thus, an apparently single crystal of xanthophyllite displays optical anormaly and pseudo-hexagonal symmetry in structure as well as in morphology.

The authors are inclined to assume that the xanthophyllite from Chichibu first crystallized out as a hypothetical high temperature form with hexagonal symmetry, and the volume change due to the transition to low temperature form brought about an imbricated stacking of thin laminae, which may have caused "apparent cleavage" of the mineral. Since the crystal structure of xanthopyllite is essentially simillar to those of micas, so-called polytypism of mica schould be re-investigated in view of those results.

Spectrographic Studies on Some Ore Minerals (Part I)
(Examination of the Working Condition)

(pp. 693-701)

Kiyoshi Takimoto and Taneo Minato

In order to select the most suitable working condition of qualitative spectrographic analysis of sulphide ore minerals for minor constituents, several experiments were performed on sphalerite and pyrite, using a Shimadzu NQM-60 Type quartz spectrograph.

Working condition discussed in the present study are as follows: (1) excitation method (comparison of comparative sensitivities for anode and cathode layer excitation), (2) gap between poles (2~4 mm.), (3) current (4~8A.-110V., D.C.), (4) depth of the sample hole of carbon electrode (1.5 ~3.0 mm.).

Sphalerite from the Shimokawa Mine, Hokkaido

(pp. 702-709)

Kenji Togari

The Shimokawa mine, which is within 7 km. south-east of the town of Shimokawa, is noted as the only working large deposit of cupriferous iron sulphide ore in Hokkaido.

The ore deposits of this mine are formed in the shear zone along the eastern margin of a diabase slate complex mass, in which cupriferous pyrite deposits have replaced both the diabase and the slate. The ore deposits belong to the category of so-called Kieslager.

The ore is composed mainly of pyrite and chalcopyrite, with a small

amount of pyrrhotite, sphalerite, cubanite and galena, and divided into compact ore and impregnated or banded ore. The samples of sphalerite for this study were taken from the compact ore.

At first samples are arranged according to the Ostwald colour standards. Next, the composition of each colour may be represented by an equation of the form C+W+B=100%, where C=full colour, W white and B=black. In this manner, the relation between hue and brilliance is determined. Material becomes darker in accordance with the increase of iron. Besides there is a tendency among sphalerites to get paler in colour in relation to the contents of minor elements.

Among minor elements Fe, Pb and Cu are rather plentiful and distributed in wide area, but Co, Ni and Mn, only partially. Ag, Sn and Pd are found in the central part of the ore body, while Bi, Te and Ga, in the marginal part.

On the Chemical Properties, Optical Properties and the Structural Types of Some Muscovites and Phlogopites.

(pp. 710-721)

Takeshi Tomisaka

The chemical compositions, the optical properties, the d. t. a. curves, and the structural types of three specimens of mica group mineral are reported. The chemical formulae and the structural types were determined as follows. (1) Hydrous muscovite which was found in muscovite vein in serpentine rock from Maruo, Ubé City, Yamaguchi Pref.: $(K_{0.63}Na_{0.12}Ca_{0.02})_{0.77}(H_3O)_{0.29})_{1.06}(Al^{\prime\prime\prime}_{2.08}Ti_{0.01}Fe^{\prime\prime}_{0.01}Fe^{\prime\prime\prime}_{0.07}Mg_{0.05})_{2.22}(Al_{1.11}Si_{2.89})_{4.00}O_{10}(OH)_{2.00}$; $2M_1$, a=5.19Å, b=8.99Å, c=20.09Å, $\beta=95°30'$. (2) Muscovite which was found in "Roseki" deposit embedded in liparite at the Uku mine, Yamaguchi Pref.: $(K_{0.39}Na_{0.13}Ca_{0.02}(H_3O)_{0.15})_{0.91}(Al_{2.05}Fe^{\prime\prime\prime}_{0.03}Mg_{0.18})_{2.16}(Al_{1.16}Si_{2.84})_{4.00}O_{10}(OH)_{2.00}$; $2M_1$, a=5.18Å, b=9.00Å, c=20.18Å, $\beta=95°20'$. (3) Biotitic phlogopite which was found in cavities in basalt from Musturé Island, Yamaguchi Pref.: $(K_{0.82}Na_{0.31}Ca_{0.01})_{1.14}(Mg_{2.16}Fe^{\prime\prime}_{0.16}Fe^{\prime\prime\prime}_{0.18}Mn_{0.01}Ti_{0.27})_{3.01}(Al_{0.89}Si_{2.07})_{3.86}O_{10}(OH_{1.48}F_{0.07})_{1.55}$; monoclinic three-layer structure ("3M"), a=5.30Å, b=9.24Å, c=30.56Å, $\beta=90°30'$.

The author discussed the relationship between the conditions of their

formation and the structural types on the basis of these results as well as of previous data.

The Relation between the Minute Content of Uranium in Zircon and its Mineralogical Characters

(pp. 722-737)

Yasuo Ukai, Takaya Kawakami and Yasuhiro Kimura

The uranium contents of representative zircon specimens collected from the weathered granite sands of the Tensei mine, Oosaka Pref., were analyzed by the microfluorimetric method. The radioactivity of zircon was measured by the decatron type countmeter, and it was generally proportional to the uranium content. The natural fluorescence intensity activated by the ultraviolet ray was determined by means of a sensitive photomultiplier detector, and the fluorescence intensity of zircon containing a comparatively large amount of uranium was lower than that containing smaller amount.

An attempt to find some relation between the colour and the uranium content in zircon was fruitless except for the facts that the colourless zircon was relatively low in its radioactivity while the greenish brown member was moderately high. The intensity of diffraction lines of zircon was measured with a Geiger counter diffractometer to investigate the relationship between uranium content and lattice defect of zircon, but there are some problems left behind.

Various minor elements contained in zircon were semiquantitatively determined by spectroscopic method.

The writer infered that the intrusion of granite of this district may be divided into three stages, each of them being characterized by the zircon content in the granite and the uranium content in the zircon. The first stage: the zircon content, rich; the uranium content, poor. The second stage: the zircon content, poor; the uranium content, slightly richer than in the first stage. The third stage: the zircon content, moderate; the uranium content, poor to considerably rich.

Cristobalite from the Abuta Mine in Hokkaido (pp. 738-746)

Yukitosi Urasima

Cristobalite and opal are found in the wall-roks (tuff and agglomerate) of the native sulphur and iron sulphides ore deposits, and in the disseminated limonite ore of the Abuta mine in south-western Hokkaido, while in the massive iron sulphides ore and bog iron ore silica occurs as quartz. The X-ray diffraction data show that the cristobalite is mostly α-(low) form. Its hexagonal platy crystal can be found in the electronmicrograph.

It is considered that the cristobalite has been formed as a secondary mineral from opal which is one of the hydrothermal alteration minerals: alunite, kaolin, montmorillonite, anatase?, pyrite, marcasite, native sulphur, etc. Cristobalite is also found in the wall-rocks of the native sulphur ore deposits of the Tokushunbetsu mine and in the clay under the bog iron ore deposit of the Kutchan mine.

On the Occurrence and Paragenesis of Magnesium-Borate Minerals in Dolomite Contact Skarns (pp. 747-762)

Takeo Watanabe

In the course of study of ores of skarn type found in some dolomite granite contact aureoles, the writer discovered several new occurrences of magnesium-borate minerals such as kotoite, suanite, ludwigite, paigeite, warwickite, szaibelyite, etc. in Japan and Korea. The magenesium-borate minerals usually occur close to the contact of granitic rocks with dolomites as boron metasomatic products. The paragenesis of the borate minerals of many localities are briefly summarized. Genesis of the boron bearing minerals in the contact aureoles are discussed.

Synthetic Pyroxenes of the Acmite-Diopside System (pp. 763-769)

Kenzo Yagi

The pyroxenes of the acmite-diopside system, which shows a complete solid solution relation, have been synthesized by sintering the glasses of

the corresponding compositions. Their optical properties (refractive indices, axial angles, and extinction angles) are determined, and a new diagram is presented to show the relation between these properties and the chemical compositions. The diagram is examined by comparing with numerous natural alkalic pyroxenes, and is proved to be useful for determinative purpose.

Of the unit cell dimensions determined from the diffraction patterns, β, a_0 and b_0 show decrease with increasing acmite molecules, while c_0 remains more or less constant.

Common Augite from Neppu, Shiribeshi Province, Hokkaido
(pp. 770 771)

Chikara Akiba

Short prismatic crystals of common augite 3~1.5 mm. across have been found as phenocrysts in Pliocene volcanic tuff from Neppu, Shiribeshi Prov., Hokkaido. Observed forms are: *a* (100), *m* (110), *b* (010), *c* (001), *s* ($\bar{1}11$) with small *z* (021).

Communication on Minerals of Japan (Part 13)
(pp. 772-790)

Mumeikai Group

33. *Coquimbite from Kònomai Mine, Hokkaido*

Kin-ichi Sakurai, Akira Kato, Ienori Fujiyama and Takaharu Imayoshi

Coquimbite was found from an old adit of an Au-Ag vein of Kônomai Mine, Hokkaido, associated with a few hydrous suphate minerals. The colour varies from whitish purple, purple to reddish purple. The crystal displays hexagonal platy or prismatic form composed of *c*(0001) and *m* (10$\bar{1}$0) with rare small faces *a*(11$\bar{2}$0) and *r*(10$\bar{1}$1). It was identified in the light of chemical analysis and X-ray study.

34. *Voltaite from Konomai Mine, Hokkaido*

Kin-ichi Sakurai, Akira Kato, Ienori Fujiyama
and Takaharu Imayoshi

Voltaite from the same locality grows on coquimbite as small black crystals with o(111) and a(100) as principal faces, and d(110). The identification was based on the optical character (n=1.600), chemical analysis and X-ray study

35. *Roemerite from Kônomai Mine, Hokkaido*

Kin-ichi Sakurai, Akira Kato, Ienori Fujiyama
and Takaharu Imayoshi

Roemerite from the same locality forms an aggregate of small chest nut brown platy crystals. The identification was also based on the chemical and X-ray characters.

36. *Xenotime from Takehara, Mié Prefecture*

Kin-ichi Sakurai, Shigeru Tabata
and Akira Kato

Xenotime from Takehara, Mié Prefecture, was found in granite pegmatite associated with monazite and zircon.

There are some varieties in colour and crystal form.

1. Bluish grey pyramidal crystal with z(101) as principal face accompanied by a(100) and τ(121). Parallel growth with zircon is common.
2. Dark grey one occurring in radial aggregate.
3. Greyish green aggregates. Rarely, pyramidal crystal with z (101). It was identified by X-ray powder data.

37. *Monazite and Fergusonite from Takehara, Mié Prefecture*

Kin-ichi Sakurai, Shigeru Tabata
and Akira Kato

Monazite from Takehara, Mié Prefecture, is brownish grey in colour and of prismatic or platy crystal with *a*(100), *m*(110), *v*(111) as principal faces, and sometimes with *n*(120), *c*(001), *w*(101) and *x*(201).

Fergusonite from the same locality is brownish black in colour. Its crystal is usually granular, and rarely prismatic with *s*(111) and *g*(320), attaining 10×3.5 mm. in size.

Mineralogical Society of Japan

OFFICERS FOR 1958–1959

President: Teiichi Ito, University of Tokyo, Tokyo.

Vice-President: Bumpei Yoshiki, Asahi Glass Co. Ltd., Tokyo.

Secretary: Toshio Sudo, Tokyo University of Education, Tokyo. Keiichi Omori, Tohoku University, Sendai.

Treasurer: Tokugoro Shoda, University of Tokyo, Tokyo.

Editor: Nobuo Katayama, University of Tokyo, Tokyo.

Councillors: Zyunpéi Harada; Hokkaido University, Sapporo. Keiichi Omori, Tsunehiko Takeuchi; Tohoku University, Sendai. Shuichi Iwao, Nobuo Katayama, Eiichi Minami, Hideo Minato, Ryoichi Sadanaga, Tokugoro Shoda, Seitaro Tsuboi, Takeo Watanabe; University of Tokyo, Tokyo. Toshio Sudo, Tokyo University of Education, Tokyo. Teiroku Sueno, Onoda Cement Co. Ltd., Tokyo. Ichiro Sunagawa, Geological Survey of Japan, Tokyo. Kin-ichi Sakurai, Tokyo. Ryoiti Kiriyama, University of Osaka, Osaka. Kitinosuke Henmi, Okayama University, Okayama. Yoshio Kinosaki, Hiroshima University, Hiroshima. Kameki Kinoshita, Toyofumi Yoshimura; Kyushu University, Fukuoka.

PUBLICATIONS

Kôbutsugaku Zasshi, Journal of the Mineralogical Society of Japan

A journal containing articles and reviews on mineralogy and allied sciences contributed by members of the Mineralogical Society of Japan. Published every four months, in Japanese. Sent to all members of the Society. Membership dues $2.00 annually.

Mineralogical Journal

A journal containing articles on mineralogy and allied sciences, published semi-annually in English principally. Contributions are invited from everyone. The Journal completed its first volume of six numbers in 1956. Back numbers may be obtained at $ 1.00 per single copy for the time being. The price of subscription to the second volume is $ 5.00 per volume.

Printed by "HERALD" Printing Co., Ltd.